

# A key role for transketolase-like 1 in tumor metabolic reprogramming

Santiago Diaz-Moralli<sup>1,2</sup>, Esther Aguilar<sup>1,2</sup>, Silvia Marin<sup>1,2</sup>, Johannes F. Coy<sup>3,4</sup>, Mieke Dewerchin<sup>5,6</sup>, Maciek R. Antoniewicz<sup>7</sup>, Oscar Meca-Cortés<sup>8</sup>, Leen Notebaert<sup>5,6</sup>, Bart Ghesquière<sup>5,6</sup>, Guy Eelen<sup>5,6</sup>, Timothy M. Thomson<sup>8</sup>, Peter Carmeliet<sup>5,6</sup>, Marta Cascante<sup>1,2</sup>

<sup>1</sup>Department of Biochemistry and Molecular Biomedicine, Faculty of Biology, Universitat de Barcelona, Barcelona, Spain

<sup>2</sup>Institute of Biomedicine of Universitat de Barcelona (IBUB) and CSIC-Associated Unit, Barcelona, Spain

<sup>3</sup>Tavargenix GmbH, Frankfurt am Main, Germany

<sup>4</sup>Zyagnum AG, Frankfurt am Main, Germany

<sup>5</sup>Laboratory of Angiogenesis and Vascular Metabolism, Department of Oncology, University of Leuven, Leuven, Belgium

<sup>6</sup>Laboratory of Angiogenesis and Vascular Metabolism, Vesalius Research Center, Leuven, Belgium

<sup>7</sup>Department of Chemical and Biomolecular Engineering, Metabolic Engineering and Systems Biology Laboratory, University of Delaware, Newark, DE, USA

<sup>8</sup>Department of Cell Biology, Institute for Molecular Biology of Barcelona, National Research Council (IBMB-CSIC), Barcelona, Spain

**Correspondence to:** Marta Cascante, **email:** martacascante@ub.edu  
Peter Carmeliet, **email:** peter.carmeliet@vib-kuleuven.be

**Keywords:** tumor metabolism, metabolic reprogramming, transketolase-like 1, lipid metabolism, pentose phosphate pathway

**Received:** March 15, 2016

**Accepted:** June 13, 2016

**Published:** July 06, 2016

## ABSTRACT

**Metabolic reprogramming, a crucial cancer hallmark, shifts metabolic pathways such as glycolysis, tricarboxylic acid cycle or lipogenesis, to enable the growth characteristics of cancer cells. Here, we provide evidence that transketolase-like 1 (TKTL1) orchestrates aerobic glycolysis, fatty acid and nucleic acid synthesis, glutamine metabolism, protection against oxidative stress and cell proliferation. Furthermore, silencing of TKTL1 reduced the levels of sphingolipids such as lactosylceramide (a sphingolipid regulating cell survival, proliferation and angiogenesis) and phosphatidylinositol (which activates PI3K/Akt/mTOR signaling). Thus, in addition to its well-known roles in glucose and amino acid metabolism, TKTL1 also regulates lipid metabolism. In conclusion, our study provides unprecedented evidence that TKTL1 plays central roles in major metabolic processes subject to reprogramming in cancer cells and thus identifies TKTL1 as a promising target for new anti-cancer therapies.**

## INTRODUCTION

Because an evident feature of cancer cells is their accelerated proliferation rate, signals mediating the response to mitogenic stimuli and alterations in (proto-)oncogenes were among the first processes to be mechanistically addressed and identified in cancer. More recently, it has become evident that cancer cells must also undergo a metabolic reprogramming to sustain the abnormal growth characteristics associated with malignant

transformation [1–3]. Consequently, different metabolic genes have been proposed to function as (proto-)oncogenes [4, 5]. Among them, glucose-6-phosphate dehydrogenase (*g6pd*) and transketolase-like 1 (*tktl1*) are of special interest because they regulate the pentose phosphate pathway (PPP), which generates NADPH for redox homeostasis and lipid synthesis and balances the flux of glucose derivatives between production of pentoses for nucleotide synthesis and supply of pyruvate for TCA cycle replenishment, or lactate production [6, 7].

Transketolase (TKT) is the key enzyme of the non-oxidative PPP branch (non-oxPPP). Via genome duplication and exon skipping, higher vertebrates acquired transketolase-like 1 (TKTL1), which compared to TKT protein lacks 38 amino acid residues [8, 9]. TKTL1 is upregulated in various cancer cells and tissues [4, 5, 10–13], and TKTL1 overexpression in cancer patients is correlated with malignancy, invasiveness, therapeutic resistance and poor prognosis [11, 14–16]. TKTL1 is required for rapid growth and viability of tumor cells [17], and protects against apoptosis induced by growth factor withdrawal [18], oxidative stress [17–19], cytotoxic therapy or targeted therapies [16, 20], while TKTL1 silencing hinders cancer cell proliferation [17, 21]. *In vivo*, silencing of TKTL1 in cancer cells reduces tumor growth, while overexpression of TKTL1 has opposite effects [7, 22]. However, little is known about how TKTL1 participates in all these processes that guarantee the growth and survival of cancer cells. Apart from the aforementioned effects, TKTL1 could also have a role in the reactions of the PPP. However, the precise reaction scheme of the non-oxPPP still remains debated, as the degree and distribution of <sup>14</sup>C-isotope labeling differ from what has been predicted by the scheme of the individual reactions [23].

Unlike TKT, which catalyzes the common two-substrate reaction by using xylulose-5-phosphate (X5P) as donor and ribose-5-phosphate (R5P) as acceptor, it has been proposed that TKTL1 may perform a one-substrate reaction by converting X5P to glyceraldehyde-3-phosphate (GA3P) and acetate, similar to phosphoketolase, an enzyme that performs a similar one-substrate reaction in heterofermentative lactic acid bacteria [8, 24]. The acetate, generated in this reaction, can then be converted to acetyl-CoA (AcCoA).

Cancer cells often have increased rates of fatty acid synthesis and therefore require large amounts of AcCoA. However, the issue of the supply of AcCoA for fatty acid synthesis in glycolytic cancer cells is still unresolved, since AcCoA production from pyruvate in cancer cells is often reduced due to: i) a switch from pyruvate kinase (PK) M1 to the less active PKM2 that reduces pyruvate production [25, 26] and ii) a decreased entry of pyruvate into the TCA cycle due to inactivation of pyruvate dehydrogenase (PDH) [27], which can be compensated by the entry of pyruvate into the TCA cycle via the anaplerotic conversion to oxaloacetate by pyruvate carboxylase (PC) [28] or glutamine catabolism [29–31]. Given that, in cancer cells, the bulk of pyruvate is directed to lactate and the flux from glutamine to AcCoA is low, it is challenging to explain how the large amounts of AcCoA necessary for fatty acid synthesis are generated. We hypothesized that the one-substrate reaction catalyzed by TKTL1 may help to explain this enigma. Our findings support this hypothesis and further contribute to clarify additional mechanisms by which TKTL1 coordinates metabolic reprogramming and tumor growth.

## RESULTS

### TKTL1 contributes to overall cellular transketolase activity

As an initial approach to characterize the relevance of TKTL1 in the metabolism and growth properties of cancer cells, we analyzed 4 cell lines with variable levels of TKTL1 (THP-1 and PC-3S, high expression; HCT-116 and PC-3M, low expression). Transduction of human THP-1 leukemia cells with a lentiviral vector expressing a TKTL1-specific shRNA (THP-1<sup>KD</sup>) specifically downregulated TKTL1 (Figure 1A) but not TKT (changed by  $4.0 \pm 1.2\%$ ;  $n = 3$ ;  $p = \text{NS}$ ). siRNA-mediated silencing reduced TKTL1 expression by  $86 \pm 13\%$  in human PC-3S prostate cancer cells, by  $81 \pm 13\%$  in human PC-3M prostate cancer cells and by  $60 \pm 28\%$  in human HCT116 colorectal carcinoma cells ( $n = 5$ ;  $p < 0.01$  for all). Consistent with the contribution by both TKT and TKTL1 to the overall transketolase activity according to their relative expression [10, 32], silencing of TKTL1 lowered but did not eliminate total transketolase activity (measured as GA3P production from R5P and X5P). Indeed, total transketolase activity was reduced by 60% in THP-1<sup>KD</sup> cells (Figure 1B) and by 37% in PC-3S<sup>KD</sup> cells (mU/mg protein:  $8.0 \pm 1.0$  in PC-3S<sup>WT</sup> cells *versus*  $5.0 \pm 0.4$  in PC-3S<sup>KD</sup> cells;  $n = 3$ ;  $p < 0.05$ ), but not in HCT116<sup>KD</sup> or PC-3M<sup>KD</sup> cells (changed by  $7 \pm 1\%$  in HCT116<sup>KD</sup> cells and by  $1 \pm 3\%$  in PC-3M<sup>KD</sup> cells;  $n = 5$ ;  $p = \text{ns}$ ), indicating that TKTL1 minimally contributed to the transketolase activity in the latter cells.

Proliferation of THP-1<sup>KD</sup> cells was reduced by  $21 \pm 4\%$  ( $n = 4$ ;  $p < 0.005$ ). In PC-3S<sup>KD</sup> cells, TKTL1 silencing substantially affected viability, decreasing the cell population by  $51 \pm 12\%$  ( $n = 6$ ;  $p < 0.01$ ) 96 hours after siRNA treatment. Interestingly, despite the minimal contribution of TKTL1 to the transketolase activity, proliferation was also reduced by  $16 \pm 5\%$  ( $n = 6$ ;  $p < 0.005$ ) in HCT116<sup>KD</sup> cells and by  $21 \pm 1\%$  in PC-3M<sup>KD</sup> cells ( $n = 3$ ;  $p < 0.001$ ), suggesting that TKTL1 affected cell proliferation independently of its transketolase activity. For the remainder of the study, we have used THP-1<sup>KD</sup> and HCT116<sup>KD</sup> cells as representative cells, in which TKTL1 did (THP-1<sup>KD</sup>) or did not (HCT116<sup>KD</sup>) contribute to total transketolase activity.

### The transketolase activity of TKTL1 drives glucose metabolism

Glucose consumption and lactate production were reduced by 34% and 66% in THP-1<sup>KD</sup> cells (Figure 1C, 1D). Even when considering alanine synthesized from pyruvate, the total production of lactate plus alanine was reduced by 64% (Figure 1D). Furthermore, the lactate production *vs.* glucose consumption ratio was  $1.1 \pm 0.1$  in THP-1<sup>KD</sup> cells and  $2.0 \pm 0.4$  in THP-1<sup>WT</sup> cells, confirming that TKTL1 levels correlate with glucose metabolism

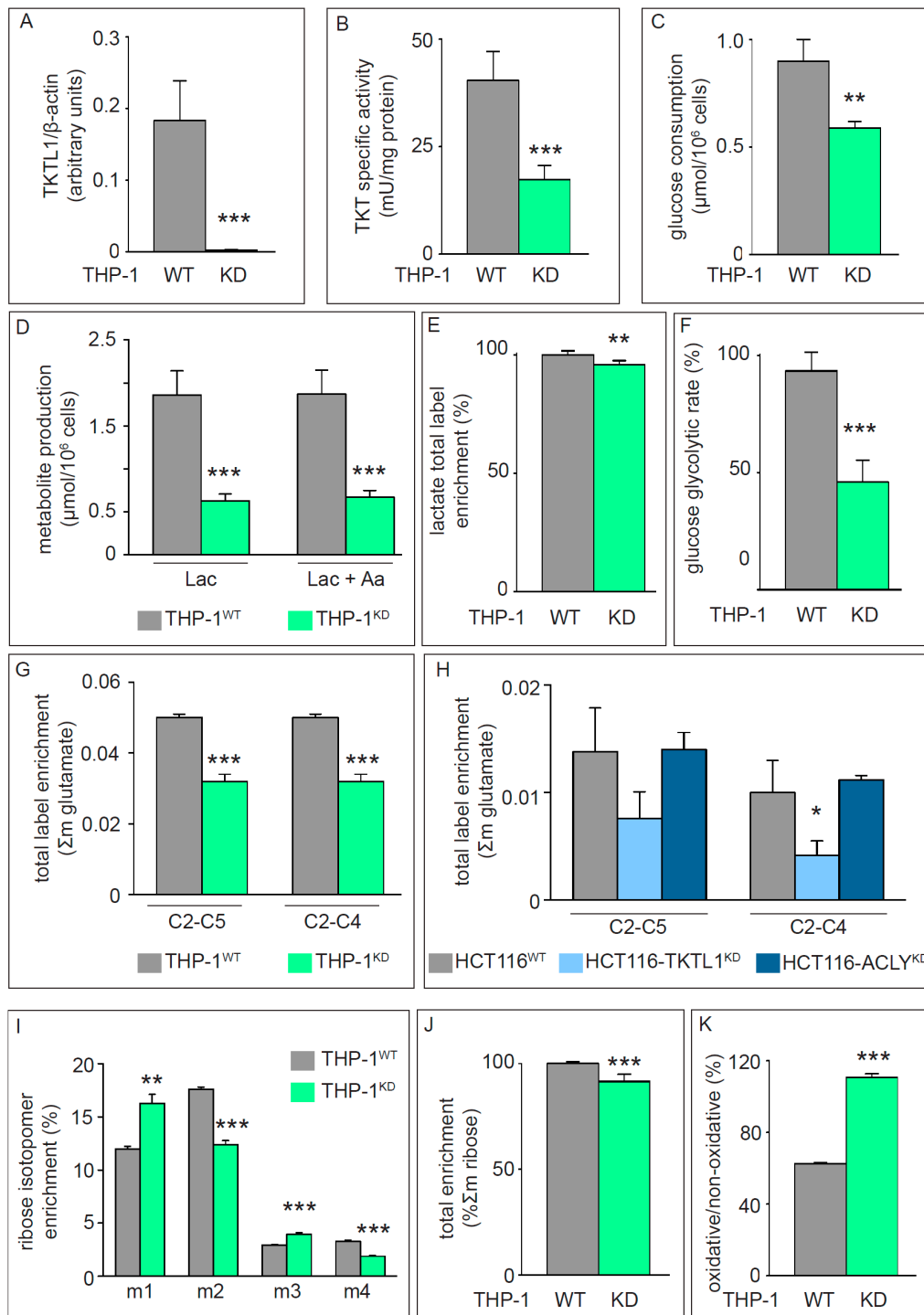


**Figure 1: Effects of TKTL1 silencing on Transketolase activity, glycolysis, TCA Cycle and PPP.** **A.** Densitometric quantification of immunoblotting for TKTL1 in THP-1<sup>WT</sup> and THP-1<sup>KD</sup> cells.  $\beta$ -Actin was used as loading control (mean $\pm$ SD; n=4; \*\*\*p<0.001). **B.** Enzymatic assay for total transketolase activity in THP-1<sup>WT</sup> and THP-1<sup>KD</sup> cells (mean $\pm$ SD; n=8; \*\*\*p<0.001). **C, D.** Glucose consumption (C) and lactate and alanine production (D) in THP-1<sup>WT</sup> and THP-1<sup>KD</sup> cells (mean $\pm$ SD; n=4; \*\*p<0.01, \*\*\*p<0.001). **E.** Total label enrichment in lactate for THP-1<sup>WT</sup> and THP-1<sup>KD</sup> cells (mean $\pm$ SD; n=4; \*\*p<0.01; values for THP-1<sup>WT</sup> were set to 100%). **F.** Glucose glycolytic rate in THP-1<sup>WT</sup> and THP-1<sup>KD</sup> cells (mean $\pm$ SD; n=4; \*\*\*p<0.001). **G, H.** Label enrichment of fragments C2-C5 and C2-C4 of glutamate in THP-1<sup>WT</sup> and THP-1<sup>KD</sup> cells (mean $\pm$ SD; n=6; \*\*\*p<0.001) (G) and in HCT116<sup>WT</sup>, HCT116-TKTL1<sup>KD</sup> and HCT116-ACLY<sup>KD</sup> cells (mean $\pm$ SD; n=3; \*p<0.05) (H). **I.** RNA ribose isotopologue distribution of <sup>13</sup>C enrichment in THP-1<sup>WT</sup> and THP-1<sup>KD</sup> cells (mean $\pm$ SD; n=3; \*\*p<0.01, \*\*\*p<0.001). **J.** Total <sup>13</sup>C RNA ribose enrichment calculated as  $\Sigma m = m1+m2+m3+m4+m5$  in THP-1<sup>WT</sup> and THP-1<sup>KD</sup> cells (mean $\pm$ SD; n=5; \*\*\*p<0.001; values for THP-1<sup>WT</sup> were set to 100%). **K.** Contribution of the oxPPP versus non-oxPPP, calculated as (m1/m2) (mean $\pm$ SD; n=3; \*\*\*p<0.001). See also Figure 2 and Figure 4.

and the Warburg effect [33]. [1,2-<sup>13</sup>C<sub>2</sub>]-glucose-based metabolic flux analysis confirmed that TKTL1 silencing reduced total lactate label enrichment (Figure 1E) and the glucose glycolytic rate (% of glucose converted to lactate and alanine, via glycolysis) by 45% in THP-1<sup>KD</sup> cells (Figure 1F), indicating that the total amount and fraction of glucose consumed through glycolysis were reduced and that other uses of carbons from glucose were enhanced.

We measured the rate of glucose oxidation by analyzing the enrichment of [1,2-<sup>13</sup>C<sub>2</sub>]-glucose in two <sup>13</sup>C-glutamate fragments, i.e. carbons 2 to 5 (C2-C5) and carbons 2 to 4 (C2-C4). Label incorporation into glutamate ( $\Sigma m$ : glutamate enrichment) was reduced in THP-1<sup>KD</sup> cells (Figure 1G). To estimate the role of PDH and pyruvate carboxylase (PC) in regulating the entry of glycolytic intermediates into the TCA cycle, we measured the PDH/PC ratio, whereby the PDH activity was measured as  $[m2(C2-C5) - m2(C2-C4)]/m2(C2-C5)$  and the PC activity as  $m2(C2-C4)/m2(C2-C5)$  [34]. Entry of pyruvate into the TCA cycle occurred primarily (80%) via the PDH pathway, but TKTL1 silencing did not, or only very modestly, affect the PDH/PC ratio in THP-1<sup>KD</sup> cells (Figure 2A, 2B).

In HCT116<sup>KD</sup> cells, in which TKTL1 did not significantly contribute to the overall transketolase

activity, no differences in glucose consumption, lactate production (not shown), glucose oxidation (Figure 1H) or PDH/PC activities (Figure 2C, 2D) were observed. Thus, TKTL1 drives the glucose metabolism and contributes to the Warburg effect in cancer cells through its transketolase activity.

### TKTL1 contributes to the non-oxidative pentose phosphate pathway

We analyzed the role of TKTL1 in regulating the incorporation of glucose in the PPP by measuring metabolic fluxes via isotopomer analysis (Figure 3). After [1,2-<sup>13</sup>C<sub>2</sub>]-glucose incubation, the PPP flux was determined by measuring ribose enrichment: [1,2-<sup>13</sup>C<sub>2</sub>]-glucose generates m1 ribose if metabolized through the oxidative branch (oxPPP), whereas it produces m2 ribose via the non-oxPPP. Further recombination of labeled intermediates leads to m3 (oxPPP) and m4 (non-oxPPP) ribose. In THP-1<sup>KD</sup> cells, TKTL1 silencing increased the pool of m1 and m3 ribose, while decreasing the pool of m2 and m4 ribose, indicating that the non-oxPPP flux was reduced (Figure 1I). Moreover, the decrease in total enrichment of ribose indicated that TKTL1 silencing reduced the net PPP flux by 10% (Figure 1J) and that the

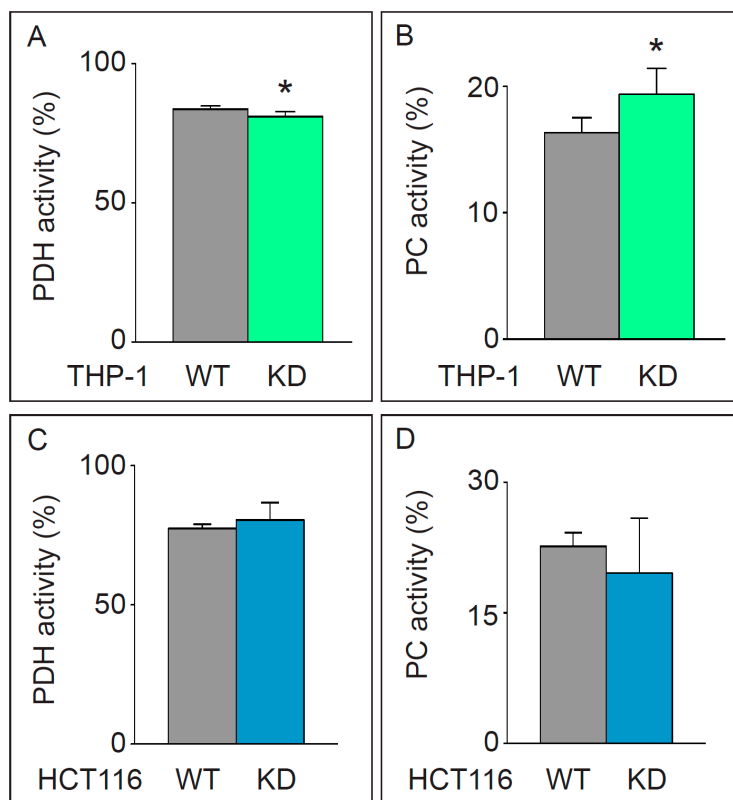


**Figure 2: Analysis of glutamate enrichment.** A, B. Pyruvate dehydrogenase (PDH) (mean±SD; n=6; \*p<0.05) (A) and pyruvate carboxylase (PC) activity (mean±SD; n=6; \*p<0.05) (B) in THP-1<sup>WT</sup> and THP-1<sup>KD</sup> cells. C, D. Pyruvate dehydrogenase (PDH) (mean±SD; n=4; p=NS) (C) and pyruvate carboxylase (PC) activity (mean±SD; n=4; p=NS) (D) in HCT116<sup>WT</sup> and HCT116-TKTL1<sup>KD</sup> cells.

relative contribution of the oxPPP over the non-oxPPP flux, calculated as m1/m2, was increased in THP-1<sup>KD</sup> cells (Figure 1K). Phase plane analysis of normalized m1 and m2 ribose isotopologues graphically illustrates these results (Figure 4A). Interestingly, similar results were obtained in HCT116<sup>KD</sup> cells (Figure 4B), even though TKTL1 does not contribute to the total transketolase activity in these cells.

### TKTL1 silencing enhances glutamine consumption

In addition to glucose, glutamine is a major source of carbon atoms for the cell, anaplerotically replenishing

the TCA cycle to maintain an active mitochondrial metabolism when pyruvate supply is compromised and enabling the production of AcCoA either through the TCA cycle or by forming citrate via reductive carboxylation [30, 31]. TKTL1 silencing in THP-1<sup>KD</sup> cells did not affect glutamate accumulation or glutamine consumption (Figure 4C, 4D). In contrast, TKTL1 silencing in HCT116<sup>KD</sup> cells increased glutamate and glutamine consumption (Figure 4E, 4F). However, even though glucose and glutamine metabolism were modulated differently in THP-1 and HCT116 cells, TKTL1 silencing induced similar changes in the ratio of glucose/glutamine consumption rates in both cell lines. This ratio was decreased by 19% in THP-1<sup>KD</sup> cells and by 25% in HCT116<sup>KD</sup> cells, indicating

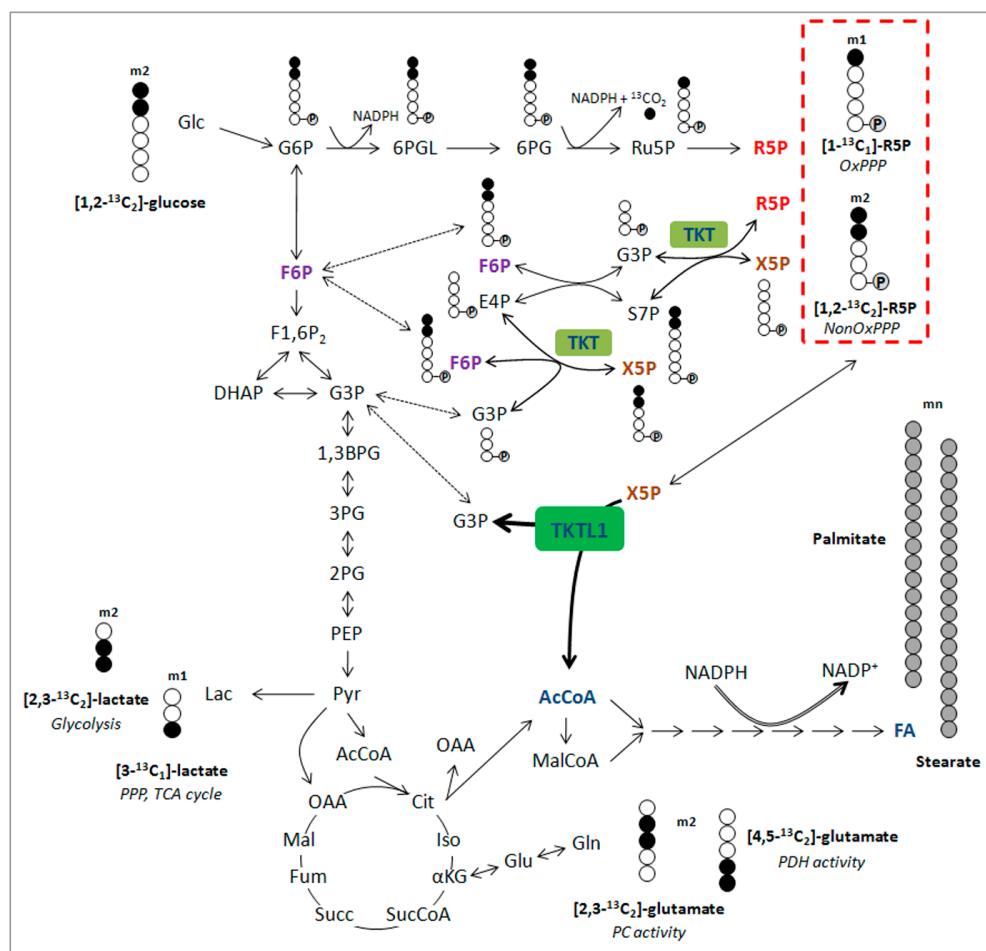


**Figure 3: Overview of isotopomer formation through carbon distribution of [1,2-<sup>13</sup>C<sub>2</sub>]-glucose.** Distribution of carbon atoms from [1,2-<sup>13</sup>C<sub>2</sub>]-glucose results in the presence of different kinds of isotopomers from lactate, glutamate and ribose-5-phosphate and reflect the involvement of specific pathways (*italic*). Ribose-5-phosphate incorporating 3, 4 or 5 <sup>13</sup>C atoms (m3, m4 and m5) is generated through recirculation of labeled molecules in the PPP. Carbons are represented by circles. Filled circles represent carbons that have incorporated label from [1,2-<sup>13</sup>C<sub>2</sub>]-glucose, open circles represent unlabeled carbons. Circles containing P represent phosphate groups. Abbreviations: m1, m2, isotopologues; 1,3BPG, 1,3-bisphosphoglycerate; 2PG, 2-phosphoglycerate; 3PG, 3-phosphoglycerate; 6PG, 6-phosphogluconate; 6PGL, 6-phosphogluconolactone; AcCoA, acetyl-CoA; Cit, citrate; DHAP, dihydroxyacetone phosphate; E4P, erythrose-4-phosphate; FA, fatty acids; F1,6P<sub>2</sub>, fructose-1,6-bisphosphate; F6P, fructose-6-phosphate; Fum, fumarate; G3P, glyceraldehyde-3-phosphate; Glc, glucose; G6P, glucose-6-phosphate; Iso, isocitrate; Lac, lactate; Mal, malate; MalCoA, malonyl-CoA; OAA, oxaloacetate; PEP, phosphoenolpyruvate; Pyr, pyruvate; R5P, ribose-5-phosphate; Ru5P, ribulose-5-phosphate; S7P, sedoheptulose-7-phosphate; Succ, succinate; SucCoA, succinyl-CoA; X5P, xylulose-5-phosphate; αKG, α-ketoglutarate.

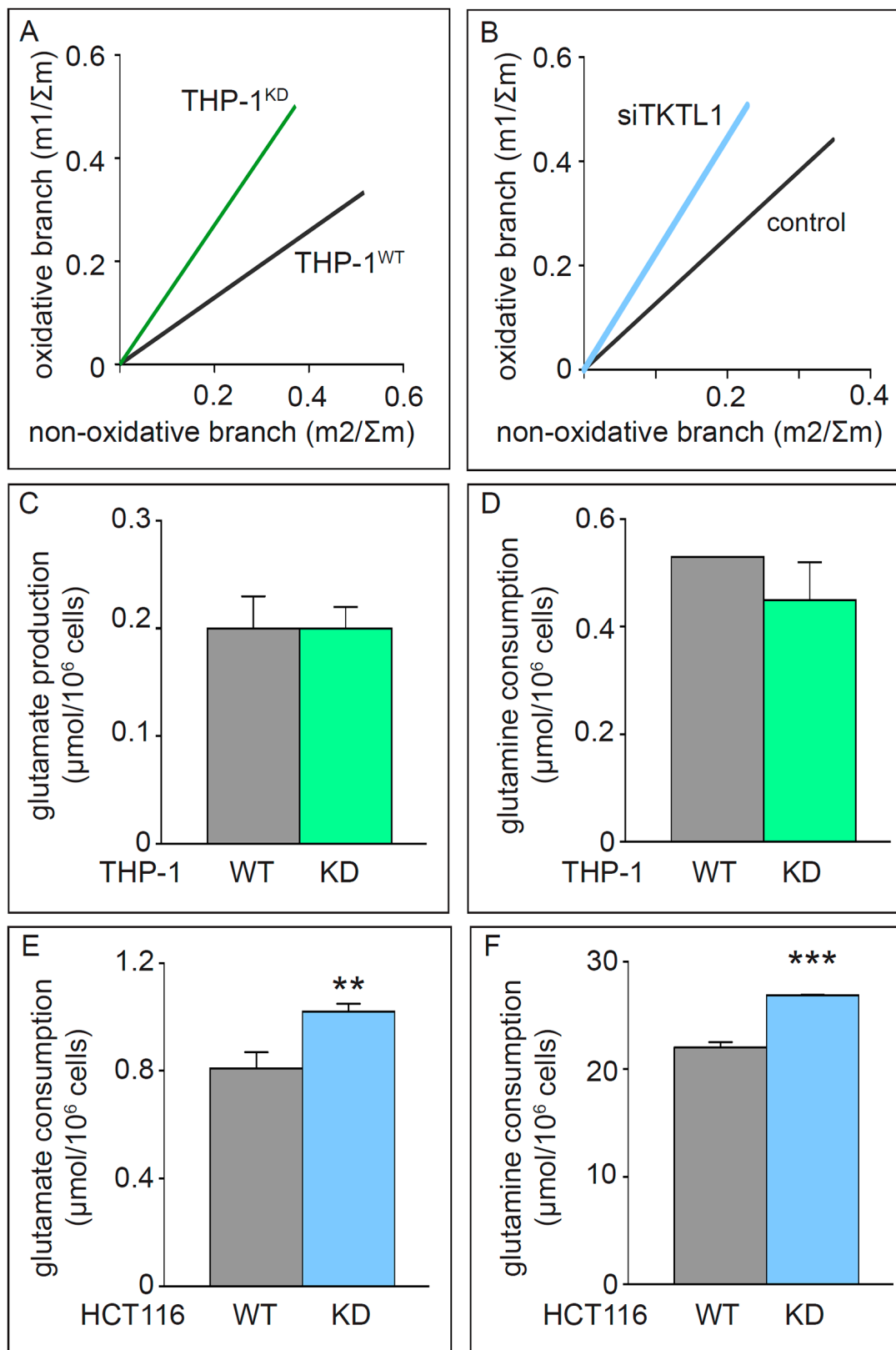


**Figure 4: Effects of TKTL1 silencing on PPP unbalance and glutamine metabolism.** A, B. Phase plane analyses of ribose isotopologues m1 and m2 normalized to  $\Sigma m$  in THP-1<sup>WT</sup> and THP-1<sup>KD</sup> cells (A) and of ribose isotopologues in HCT116 cells treated with control siRNA (control) and anti-TKTL1 siRNA (siTKTL1) (B). C, D. Glutamate accumulation (C) and glutamine consumption (D) in THP-1<sup>WT</sup> and THP-1<sup>KD</sup> cells (mean $\pm$ SD; n=3; p=NS). E, F. Glutamate accumulation (E) and glutamine consumption (F) in HCT116<sup>WT</sup> and HCT116-TKTL1<sup>KD</sup> cells (mean $\pm$ SD; n=3; \*\*p<0.01, \*\*\*p<0.001).

that TKTL1 regulates the balance between glucose and glutamine metabolism regardless of how it modulates each of these metabolic pathways individually or the extent of its contribution to overall transketolase activity.

On the other hand, THP-1<sup>KD</sup> cells reduced the consumption of isoleucine (Ile), leucine (Leu) and valine (Val), i.e. amino acids that are also catabolized to replenish the TCA cycle and generate AcCoA (Figure 5), indicating that TKTL1 favors these AcCoA production pathways.

### TKTL1 contributes to fatty acid synthesis

Given the importance of fatty acid synthesis in rapidly proliferating cells and the role of TKTL1 silencing on several pathways leading to AcCoA production, we analyzed whether TKTL1 silencing affects lipid synthesis. We determined [1,2-<sup>13</sup>C<sub>2</sub>]-glucose incorporation in C16-palmitate and C18-stearate as a surrogate read-out of [1,2-<sup>13</sup>C<sub>2</sub>]-glucose incorporation into AcCoA, and measured the fraction of *de novo* synthesized lipids (FNS) and the proportion of lipids synthesized by chain elongation. FNS levels and the contribution of [1,2-<sup>13</sup>C<sub>2</sub>]-glucose to fatty acid synthesis were reduced in THP-1<sup>KD</sup> cells (Figure 6A, 6B), indicating that TKTL1 participated in the conversion of glucose carbon into fatty acids via generation of AcCoA. Similar effects were observed in HCT116<sup>KD</sup> cells (Figure 6C, 6D). The decreased contribution of glucose to lipid synthesis was not attributable solely to a slower growth rate, since the incorporation of [1,2-<sup>13</sup>C<sub>2</sub>]-glucose into fatty acids was reduced more than the [1,2-<sup>13</sup>C<sub>2</sub>]-glucose incorporation into nucleotides (Table 1).

### TKTL1 contributes to the maintenance of the global cell lipidome

We also analyzed the lipidome by UPLC/MS and assigned > 200 lipid species: ~140 belonged to

11 groups of phospholipids (PL) (Table 2), of which phosphatidylcholines (PCs) (including the abundant PC 32:1 and PC 34:1 species), phosphatidylethanolamines (PEs), and phosphatidylinositols (PI) were reduced in THP-1<sup>KD</sup> cells (Figure 6E-6G; Table 2). An additional 60 lipids were classified into 8 groups of sphingolipids (SL) (Table 3), of which ceramides (Cer) and lactosylceramides (LacCer) were reduced in THP-1<sup>KD</sup> cells (Figure 6H, 6I). Thus, TKTL1 not only participates in lipid synthesis but also in maintaining the global cell lipidome.

### Evidence in support of one-substrate activity by TKTL1

We explored if TKTL1 might display one-substrate activity by isotopologue analysis of m1 lactate, as this provides insight into the TKT/TKTL1-dependent glucose carbon flux through the PPP. We considered two possibilities: (i) both TKT and TKTL1 catalyze only the two-substrate reaction (Figure 7A), and (ii) TKT catalyzes the two-substrate reaction while TKTL1 catalyzes the one-substrate reaction (Figure 7B). To test this model, we analyzed the enrichment of [1,2-<sup>13</sup>C<sub>2</sub>]-glucose in m1 lactate, which can only be generated in the PPP via the two-substrate reaction, since the label is donated to AcCoA in the one-substrate reaction (Figure 4B, red pathway). Hence, in THP-1 cells, where TKTL1 accounts for 60% of the overall transketolase activity, TKTL1 silencing should *decrease* m1 lactate levels if it would only have the classical two-substrate activity (Figure 7A), but should *increase* m1 lactate levels if it had one-substrate activity (Figure 7B) since phosphorylated pentoses would be metabolized only via TKT generating more m1 lactate molecules.

This analysis revealed that the levels of m1 lactate were increased by 13 ± 7% (n = 6; p < 0.005) in THP-1<sup>KD</sup> cells, which perfectly fits with theoretical predictions for the one-substrate reaction model (Figure 7B). In HCT116

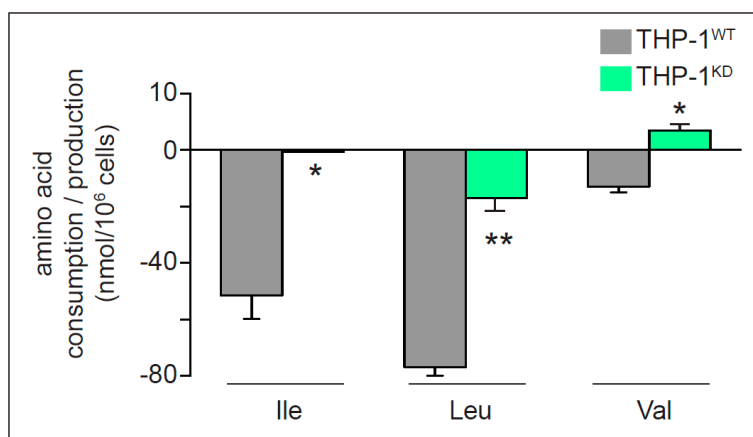


**Figure 5: Impact of TKTL1 knock down on amino acid levels.** Amino acid (AA) levels in WT and TKTL1<sup>KD</sup> THP-1 cells; positive values reflect amino acid production whereas negative values reflect AA consumption (mean±SD; n=3; \*p<0.05, \*\*p<0.01).

cells, TKTL1 silencing decreased m1 lactate levels by  $46 \pm 10\%$  ( $n = 4$ ;  $p < 0.001$ ). Given that TKTL1 minimally contributed to the overall transketolase activity in these cells, the effects on m1 lactate are unlikely to be due to its enzyme reaction but rather to the reduction of the non-oxPPP flux in TKTL1-silenced cells (Figure 4B).

### ACLY complements TKTL1 in the promotion of fatty acid synthesis

ATP-citrate lyase (ACLY) is a key enzyme regulating lipid synthesis by converting cytosolic citrate to AcCoA. To evaluate the possible role of TKTL1 in producing AcCoA in comparison with ACLY, we silenced ACLY in HCT116 (HCT116-ACLY<sup>KD</sup>) cells. SiRNA-mediated silencing reduced ACLY transcript levels by  $45 \pm 10\%$  ( $n = 4$ ;  $p < 0.001$ ) without affecting proliferation, glucose consumption or lactate production (Figure 8A-8C), or altering the glycolytic rate or the PC/PDH ratio (not shown). ACLY silencing did not affect glutamate levels or glutamine consumption (not shown), nor did it alter glutamate enrichment (Figure 1H), but decreased fatty acid enrichment (Figure 6D), as expected. Indeed, when ACLY's activity is reduced, less citrate is processed to generate AcCoA and fewer labeled substrates are incorporated into palmitate without however affecting stearate enrichment (Figure 6D). These results, together

with the abovementioned results in TKTL1 silenced cells, suggest that ACLY and TKTL1 play cooperative roles in fatty acids synthesis.

## DISCUSSION

In this study, we have found that TKTL1 plays broader roles in cell metabolism than previously anticipated. First, in agreement with previous data [7], we show that TKTL1 enhances glycolysis and sustains accelerated proliferation. These findings implicate TKTL1 in aerobic glycolysis (Warburg effect), the mechanism on which cancer and other proliferative cells rely to produce glycolytic intermediates for biomass synthesis and energy [25, 26, 35, 36]. TKTL1 also enhances the PPP flux for biosynthetic reactions, as the PPP generates ribose-5-phosphate for nucleic acid synthesis and NADPH for fatty acid synthesis and maintaining redox homeostasis to protect cells against apoptosis [37].

Second, TKTL1 affects glutamine metabolism, the other main carbon source in cancer cells. In contrast to its effects on glucose metabolism, we show that depletion of TKTL1 enhances glutamine consumption rates independent of its transketolase activity. Interestingly, the effect of TKTL1 on the ox-PPP *versus* non-ox PPP ratio is also independent of its contribution to the overall transketolase activity. Given that both glutaminolysis and

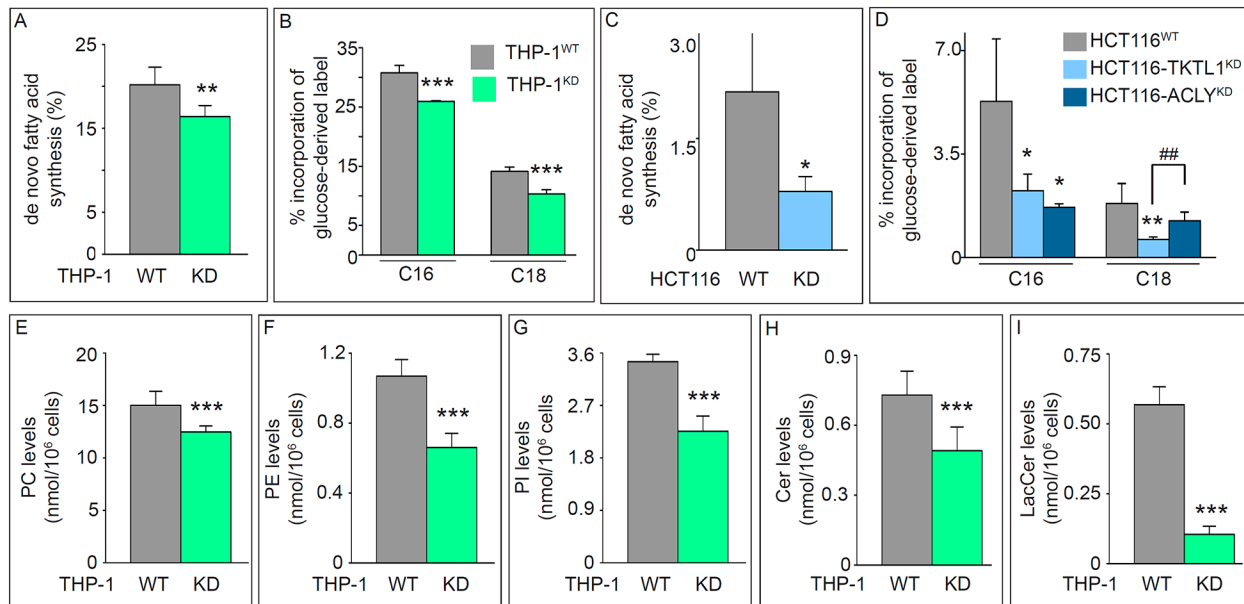


**Figure 6: Effects of TKTL1 silencing on global cell lipidome.** A, B. Fraction of *de novo* synthesis of fatty acids (FNS) (mean±SD;  $n=6$ ;  $**p<0.01$ ) (A) and percentage of label incorporation from glucose into palmitate (C16) and stearate (C18) (mean±SD;  $n=5$ ;  $***p<0.001$ ) (B) in THP-1<sup>WT</sup> and THP-1<sup>KD</sup> cells. C, D. Fraction of *de novo* synthesis of fatty acids (FNS) (mean±SD;  $n=4$ ;  $*p<0.05$ ) (C) and percentage of label incorporation from glucose into palmitate (C16) and stearate (C18) (mean±SD;  $n=4$ ;  $*p<0.05$ ,  $**p<0.01$ ,  $###p<0.01$ ) (D) in HCT116<sup>WT</sup>, HCT116-TKTL1<sup>KD</sup> and HCT116-ACLY<sup>KD</sup> cells. E-I. Quantification of phospholipid (E-G) and sphingolipid (H, I) content in THP-1<sup>WT</sup> and THP-1<sup>KD</sup> cell lines by UPLC-MS (mean±SD;  $n=7$ ;  $***p<0.001$ ). PC, phosphatidylcholine (E); PE, phosphatidylethanolamine (F); PI, phosphatidylinositol (G); Cer, ceramide (H); LacCer, lactosylceramide (I). See also Tables 2 and 3.



**Table 1: Label incorporation from glucose into the fatty acids palmitate and stearate**

Incorporation of glucose label into (ratio):	THP-1 cells		HCT116 cells	
	WT	KD	WT	KD
palmitate <i>versus</i> nucleotides	0.89 ± 0.01	0.82 ± 0.01***	0.17 ± 0.04	0.06 ± 0.02**
stearate <i>versus</i> nucleotides	0.40 ± 0.03	0.33 ± 0.02*	0.032 ± 0.004	0.017 ± 0.003**

Label incorporation of glucose in palmitate and stearate was compared to label incorporation in nucleotides in THP-1 and HCT116 cell (WT or silenced for TKTL1) (mean±SD; n=4; p-values are adjusted using a Holm method, \*p<0.05, \*\*p<0.01, \*\*\*p<0.005). The values represent the ratio of the incorporation of glucose label into palmitate/ stearate *versus* incorporation of glucose label into nucleotides.

**Table 2: Effect of TKTL1 knock down on phospholipid synthesis in THP-1 cells**

Species	Chain length (R)	THP-1 <sup>WT</sup>	THP-1 <sup>KD</sup>
Phosphatidyl-cholines (PC)	31:0	369 ± 24	438 ± 11.5
	32:2	285 ± 44	173 ± 29.8
	32:1	3533 ± 463	3008 ± 243
	32:0	1131 ± 67	888 ± 150
	33:3	64.1 ± 11.6	30.1 ± 4.1
	34:4	147 ± 20.9	172 ± 4.7
	34:4•	15.7 ± 2,8	9.33 ± 0.4
	34:3	53.3 ± 5.0	44.8 ± 8.3
	34:2	1422 ± 167	1249 ± 74.8
	34:1	3624 ± 861	3362 ± 604
	35:4	116 ± 18	55.8 ± 4.0
	35:2	99.7 ± 29.8	59.2 ± 8.4
	35:1	306 ± 45	208 ± 24.1
	36:6	9.64 ± 2.8	4.54 ± 1.2
	36:5	37.0 ± 9.0	20.0 ± 5.0
	36:4	147 ± 29	91.2 ± 14.4
	36:3	356 ± 53	236 ± 25
	36:2	1543 ± 187	1128 ± 241
	36:1	1282 ± 128	1302 ± 115
	37:0	5.24 ± 1.3	6.32 ± 2.6
38:8	1.40 ± 0.6	0.74 ± 0.1	
38:7	4.67 ± 0.7	2.20 ± 0.2	
38:6	52.2 ± 17.5	33.0 ± 9.2	
38:5	101 ± 16	44.3 ± 2.5	
38:4	70.2 ± 11	48.7 ± 3.8	
38:4•	72.2 ± 7.6	93.9 ± 18.3	

(Continued)

Species	Chain length (R)	THP-1 <sup>WT</sup>	THP-1 <sup>KD</sup>	
	38:3	97.8 ± 5.1	51.1 ± 16.0	
	38:3•	34.2 ± 8.2	17.3 ± 3.7	
	38:2	350 ± 114	120 ± 98.3	
	38:0	8.33 ± 4.2	7.28 ± 1.4	
	40:7	22.1 ± 10.9	11.1 ± 6.0	
	40:6	9.94 ± 4.0	6.67 ± 1.9	
	40:6•	12.7 ± 6.5	9.72 ± 1.7	
	40:5	30.4 ± 17.8	17.0 ± 7.5	
	40:2	27.1 ± 3.8	33.4 ± 3.4	
	40:2•	59.6 ± 3.3	36.4 ± 5.0	
	42:2	75.5 ± 5.3	49.4 ± 2.1	
	42:2•	31.5 ± 4.1	22.7 ± 4.1	
	44:3	17.7 ± 9.2	8.80 ± 2.7	
	44:2	33.4 ± 24.1	9.99 ± 0.6	
	44:2•	14.8 ± 9.0	13.1 ± 2.5	
	44:1	64.5 ± 44.5	48.4 ± 7.7	
	46:1	5.03 ± 3.1	4.48 ± 1.6	
	<b>TOTAL</b>	<b>15033 ± 1319</b>	<b>12481 ± 560 **</b>	
<b>Phosphatidyl-choline-plasmalogens (PC-pmg)</b>	34:2	16.7 ± 4.3	30.3 ± 6.5	
	34:1	135 ± 12	171 ± 21	
	34:0	1212 ± 139	1415 ± 137	
	36:4	37.5 ± 7.5	36.6 ± 2.9	
	36:3	11.7 ± 4.5	23.2 ± 3.0	
	36:3•	33.1 ± 5.7	45.9 ± 7.9	
	36:2	53.9 ± 0.7	25.6 ± 0.5	
	36:2•	46.7 ± 5.0	-	
	36:1	138 ± 5.7	77 ± 55	
	36:1•	57.9 ± 13.5	14.8 ± 3.2	
	36:0	263 ± 38	204 ± 97	
	38:6	231 ± 33	179 ± 5.8	
	38:5	29.9 ± 7.9	30.4 ± 5.8	
	40:7	9.68 ± 2.6	6.00 ± 1.4	
	40:6	18.4 ± 1.0	7.77 ± 1.8	
		<b>TOTAL</b>	<b>1985 ± 255</b>	<b>2073 ± 454</b>
	<b>Lyso-phosphatidyl-cholines (LPC)</b>	16:1	204 ± 38	154 ± 23
16:0		570 ± 154	579 ± 255	
18:3		100 ± 9	67.3 ± 13.6	
18:2		46.8 ± 6.6	39.9 ± 9.7	

(Continued)

Species	Chain length (R)	THP-1 <sup>WT</sup>	THP-1 <sup>KD</sup>
	18:1	352 ± 44	275 ± 39
	18:0	82.0 ± 14.6	124 ± 45
	20:4	85.0 ± 15.2	60.6 ± 16.7
	20:3	12.2 ± 0.8	15.2 ± 3.5
	20:1	19.5 ± 6.2	11.3 ± 2.3
	20:0	2.25 ± 0.1	1.79 ± 0.2
	<b>TOTAL</b>	<b>1373 ± 175</b>	<b>1246 ± 281</b>
<b>Lyso-phospatidyl-choline-plasmalogens (LPC-pmg)</b>	16:1	16.7 ± 4.9	7.93 ± 3.4
	16:0	80.6 ± 29.9	130.7 ± 41
	18:1	10.5 ± 2.4	12.3 ± 2.3
	18:0	10.4 ± 2.7	6.5 ± 1.2
	<b>TOTAL</b>	<b>109 ± 25</b>	<b>153 ± 37 *</b>
<b>Phosphatidyl-ethanolamines (PE)</b>	32:2	18.8 ± 7.3	11.9 ± 7
	32:1	125 ± 25	88.2 ± 28.6
	32:0	7.49 ± 0.6	4.84 ± 1.0
	34:3	17.1 ± 6.1	9.98 ± 4.6
	34:2	126 ± 13	70.1 ± 10.2
	34:1	165 ± 21	126 ± 9.7
	36:5	40.7 ± 25.3	29.2 ± 3.1
	36:4	45.7 ± 7.7	26.9 ± 7.4
	36:3	79.4 ± 8.1	35.4 ± 10.1
	36:2	165 ± 29	84.5 ± 6.0
	36:1	100 ± 13	80.4 ± 8.8
	38:7	51.8 ± 3.7	43.9 ± 1.7
	38:6	31.2 ± 6.4	16.0 ± 2.3
	38:5	42.0 ± 11.9	20.4 ± 6.1
	38:4	65.6 ± 7.9	36.4 ± 6.7
	38:2	13.0 ± 2.6	7.3 ± 1.6
	38:1	3.63 ± 0.2	1.79 ± 0.1
	38:1•	13.5 ± 0.7	12.9 ± 0.5
	40:5	40.3 ± 9.4	24.7 ± 2.0
	<b>TOTAL</b>	<b>1069 ± 94</b>	<b>660 ± 81 ***</b>
<b>Phosphatidyl-ethanolamine-plasmalogens (PE-pmg)</b>	34:3	25.2 ± 2.9	19.9 ± 4.2
	34:2	267 ± 65	210 ± 15
	34:1	354 ± 61	268 ± 35
	36:4	141 ± 36	131 ± 9

(Continued)

Species	Chain length (R)	THP-1 <sup>WT</sup>	THP-1 <sup>KD</sup>
	36:4•	178 ± 5	159 ± 7
	36:3	67.9 ± 5.6	55.5 ± 2.9
	36:3•	69.2 ± 7.2	38.0 ± 2.3
	36:2	84.4 ± 49.1	47.5 ± 24.0
	36:2•	97.6 ± 13.9	46.0 ± 3.2
	36:1	102 ± 41	62.8 ± 6.2
	36:1•	100 ± 6	51.7 ± 3.2
	36:0	36.4 ± 9.8	26.0 ± 1.8
	38:6	72.9 ± 14.5	70.2 ± 1.9
	38:6•	113 ± 11	105 ± 5
	38:5	71.0 ± 11	84.4 ± 4.3
	38:5•	64.0 ± 1.9	57.8 ± 1.9
	38:4	37.3 ± 10.3	17.3 ± 2.1
	40:7	0.26 ± 0.45	0.73 ± 0.23
	40:6	7.22 ± 0.6	4.25 ± 0.2
	<b>TOTAL</b>	<b>1361 ± 220</b>	<b>1030 ± 89 *</b>
<b>Lyso-phosphatidyl-ethanolamines (LPE)</b>	16:1	18.8 ± 7.3	12.8 ± 2.6
	16:0	30.7 ± 8.1	27.6 ± 4.2
	18:2	15.6 ± 5.1	9.78 ± 1.5
	18:1	64.6 ± 24.7	36.7 ± 6.2
	18:0	44.4 ± 12.5	41.5 ± 4.1
	20:4	10.5 ± 3.2	6.25 ± 0.6
	20:3	8.1 ± 3.7	5.2 ± 2.3
	<b>TOTAL</b>	<b>193 ± 59</b>	<b>140 ± 11 *</b>
<b>Lyso-phosphatidyl-ethanolamine-plasmalogens (LPE-pmg)</b>	16:1	0.26 ± 0.07	0.24 ± 0.01
	16:0	84.7 ± 9.8	83.0 ± 4.4
	18:1	5.13 ± 1.7	2.98 ± 0.7
	18:0	22.3 ± 5.4	20.3 ± 1.5
	20:1	0.55 ± 0.04	0.44 ± 0.07
	20:0	1.76 ± 1.0	1.49 ± 0.4
	22:1	1.01 ± 0.1	0.74 ± 0.04
	22:0	1.13 ± 0.1	0.89 ± 0.07
<b>TOTAL</b>	<b>66.8 ± 52.5</b>	<b>61.3 ± 45.4</b>	
<b>Phosphatidyl-serines (PS)</b>	32:1	34.0 ± 6.1	59.2 ± 1.4
	34:2	13.3 ± 1.7	14.5 ± 7.9
	34:1	157 ± 43	172 ± 98
	36:5	25.0 ± 0.6	22.8 ± 0.9

(Continued)

Species	Chain length (R)	THP-1 <sup>WT</sup>	THP-1 <sup>KD</sup>
	36:2	77.7 ± 8.3	56.3 ± 28.7
	36:1	218 ± 26	167 ± 66
	38:3	41.3 ± 8.0	57.7 ± 23.0
	38:2	23.7 ± 1.8	7.16 ± 0.7
	38:1	18.2 ± 1.4	5.16 ± 0.2
	40:6	48.2 ± 5.5	54.1 ± 0.5
	40:3	3.26 ± 0.3	2.14 ± 0.3
	40:2	12.0 ± 0.6	3.02 ± 0.2
	40:1	31.8 ± 8.9	22.4 ± 14.1
	<b>TOTAL</b>	<b>621 ± 59</b>	<b>572 ± 276</b>
<b>Lyso-phosphatidyl-serines (LPS)</b>	16:1	6.77 ± 1.6	12.8 ± 1.1
	16:0	3.35 ± 1.4	4.70 ± 3.6
	18:3	12.8 ± 3.8	9.93 ± 4.7
	18:2	27.2 ± 10.1	27.1 ± 17.0
	18:1	28.3 ± 7.0	24.5 ± 15.9
	18:0	60.2 ± 22.0	67.8 ± 45.7
	20:4	14.5 ± 3.7	11.0 ± 6.4
	20:3	43.7 ± 6.6	31.8 ± 15.7
	20:2	30.0 ± 4.3	34.3 ± 20.2
	22:1	0.65 ± 0.0	0.32 ± 0.19
	22:0	2.72 ± 0.23	0.14 ± 0.25
	<b>TOTAL</b>	<b>229 ± 51</b>	<b>220 ± 132</b>
<b>Phosphatidyl-inositols (PI)</b>	34:1	795 ± 178	708 ± 157
	34:0	47.0 ± 21.8	64.3 ± 32.1
	36:4	152 ± 54	187 ± 69
	36:3	128 ± 15	110 ± 20
	36:2	697 ± 45	347 ± 53
	36:1	804 ± 109	397 ± 34
	38:4	441 ± 119	259 ± 122
	38:3	306 ± 25	114 ± 11
	40:6	462 ± 24	279 ± 24
	<b>TOTAL</b>	<b>3452 ± 121</b>	<b>2257 ± 262 ***</b>

Values are expressed as pmol/10<sup>6</sup> cells (mean±SD; n=7; p-values are adjusted using a Holm method, \*p<0.05, \*\*p<0.01, \*\*\*p<0.001). To calculate the totals ± standard deviations per lipid species, we first calculated per repeat the sums of all chain length values, and then calculated the average and standard deviation of these sums. Due to the fact that in this high-throughput analysis, a peak was not present for each chain length in every repeat, some totals listed do not equal the mathematical sum of the individual chain length values.

R, total number of carbons: total number of unsaturated acyl moieties.

• Some species are detected by two independent peaks in the MS.

**Table 3: Effect of TKTL1 knock down on sphingolipid synthesis in THP-1 cells**

Species	Chain length (R)	THP-1 <sup>WT</sup>	THP-1 <sup>KD</sup>
Ceramides (Cer)	14:1	2.43 ± 0.3	0.89 ± 0.2
	14:0	8.40 ± 1.2	3.28 ± 1.1
	16:1	8.40 ± 1.5	2.91 ± 0.8
	16:0	158 ± 23	107 ± 40
	18:1	3.99 ± 0.3	1.47 ± 0.3
	18:0	20.8 ± 3.0	11.8 ± 5.2
	20:1	0.82 ± 0.12	0.30 ± 0.12
	20:0	4.67 ± 0.4	2.59 ± 1.3
	22:1	4.52 ± 0.2	2.01 ± 0.5
	22:1•	7.30 ± 1.0	2.71 ± 0.5
	22:0	40.9 ± 5.7	25.9 ± 6.3
	24:2	11.1 ± 1.6	3.14 ± 0.8
	24:1	63.6 ± 10.5	22.2 ± 6.6
	24:1•	32.6 ± 5.9	20.9 ± 2.4
	24:0	365 ± 85	285 ± 42
		<b>TOTAL</b>	<b>729 ± 103</b>
Dihydro-ceramides (DH-Cer)	16:0	13.6 ± 2.6	6.46 ± 2.3
	18:0	2.98 ± 0.9	1.48 ± 1.4
	20:0	1.31 ± 0.2	0.78 ± 0.51
	22:0	12.0 ± 2.3	5.92 ± 2.5
	24:1	20.7 ± 11.4	12.4 ± 9.6
	24:0	60.8 ± 12.5	48.4 ± 28.5
	<b>TOTAL</b>	<b>123 ± 32</b>	<b>75.4 ± 42.9 *</b>
Sphingomyelins (SM)	14:1	4.15 ± 0.4	2.15 ± 0.6
	14:0	84.0 ± 25.7	55.9 ± 12.3
	16:1	89.3 ± 17.5	68.0 ± 8.6
	16:0	1783 ± 662	1776 ± 477
	18:1	38.6 ± 5.8	22.7 ± 3.8
	18:0•	140 ± 44	107 ± 16
	20:1	7.59 ± 2.2	3.65 ± 1.5
	20:0	34.3 ± 6.9	24.6 ± 9.9
	22:2	3.57 ± 0.4	1.56 ± 0.4
	22:1	35.8 ± 2.5	21.3 ± 7.5
	22:1•	47.7 ± 7.0	26.9 ± 4.9
	22:0	170 ± 24	125 ± 32
	24:3	6.83 ± 1.5	2.85 ± 1.1

(Continued)

Species	Chain length (R)	THP-1 <sup>WT</sup>	THP-1 <sup>KD</sup>
	24:2	67.6 ± 24.3	31.1 ± 12.2
	24:1	437 ± 122	195 ± 25
	24:1•	86.7 ± 22.5	72.1 ± 29.3
	24:0	665 ± 162	562 ± 71
	<b>TOTAL</b>	<b>3555 ± 432</b>	<b>3139 ± 474</b>
<b>Dihydro-sphingomyelins (DH-SM)</b>	14:0	11.6 ± 2.9	3.26 ± 0.7
	16:0	315 ± 104	76.8 ± 10.0
	18:0	26.7 ± 6.1	6.69 ± 2.6
	20:0	11.1 ± 2.9	3.87 ± 2.0
	22:0	50.2 ± 10.2	13.0 ± 4.8
	24:1	131 ± 46	23.9 ± 9.3
	24:0	201 ± 22	52.9 ± 14
	<b>TOTAL</b>	<b>728 ± 72</b>	<b>166 ± 23 ***</b>
<b>Glucosyl-ceramides (GlcCer)</b>	14:0	2.88 ± 0.5	2.80 ± 0.7
	16:0	71.4 ± 4.4	100 ± 8
	18:0	8.67 ± 2.1	8.45 ± 2.1
	20:0	2.21 ± 0.8	1.78 ± 0.8
	22:0	27.3 ± 8.3	30.9 ± 8.2
	24:1	18.5 ± 7.3	13.7 ± 5.2
	24:0	146 ± 27	281 ± 49
	<b>TOTAL</b>	<b>284 ± 41</b>	<b>429 ± 67 **</b>
<b>Glucosyl-dihydro-ceramides (GlcDH-Cer)</b>	16:0	17.7 ± 4.7	8.4 ± 2.6
	18:0	1.78 ± 0.4	0.66 ± 0.43
	20:0	1.45 ± 0.1	0.66 ± 0.43
	22:0	12.4 ± 1.4	4.63 ± 1.3
	24:0	56.5 ± 10.4	38.5 ± 7.6
	<b>TOTAL</b>	<b>87.9 ± 10.4</b>	<b>57.1 ± 16.3 **</b>
<b>Lactosyl-ceramides (LacCer)</b>	16:0	214 ± 19	33.5 ± 4.5
	18:0	23.3 ± 3.9	1.94 ± 0.5
	20:0	6.81 ± 0.7	0.65 ± 0.45
	22:0	53.6 ± 23.0	8.38 ± 5.5
	24:1	51.1 ± 23.0	3.74 ± 0.9
	24:0	224 ± 36	57.2 ± 18.0
	<b>TOTAL</b>	<b>569 ± 64</b>	<b>105 ± 29 ***</b>
<b>Lactosyl-dihydro-ceramides (LacDH-Cer)</b>	16:0	46.1 ± 10.0	1.31 ± 0.5
	18:0	5.32 ± 0.9	-
	20:0	2.47 ± 1.3	-
	22:0	25.7 ± 11.7	0.97 ± 0.77

(Continued)

Species	Chain length (R)	THP-1 <sup>WT</sup>	THP-1 <sup>KD</sup>
	24:1	23.7 ± 11.7	3.49 ± 4.2
	24:0	91.8 ± 43.3	8.64 ± 4.3
	<b>TOTAL</b>	<b>195 ± 60</b>	<b>14.4 ± 8.9 ***</b>

Values are expressed as pmol/10<sup>6</sup> cells (mean±SD; n=7; p-values are adjusted using a Holm method, \*p<0.05, \*\*p<0.01, \*\*\*p<0.001). To calculate the totals ± standard deviations per lipid species, we first calculated per repeat the sums of all chain length values, and then calculated the average and standard deviation of these sums. Due to the fact that in this high-throughput analysis, a peak was not present for each chain length in every repeat, some totals listed do not equal the mathematical sum of the individual chain length values.

R, total number of carbons; total number of unsaturated acyl moieties.

\* Some species are detected with two independent peaks in the MS.

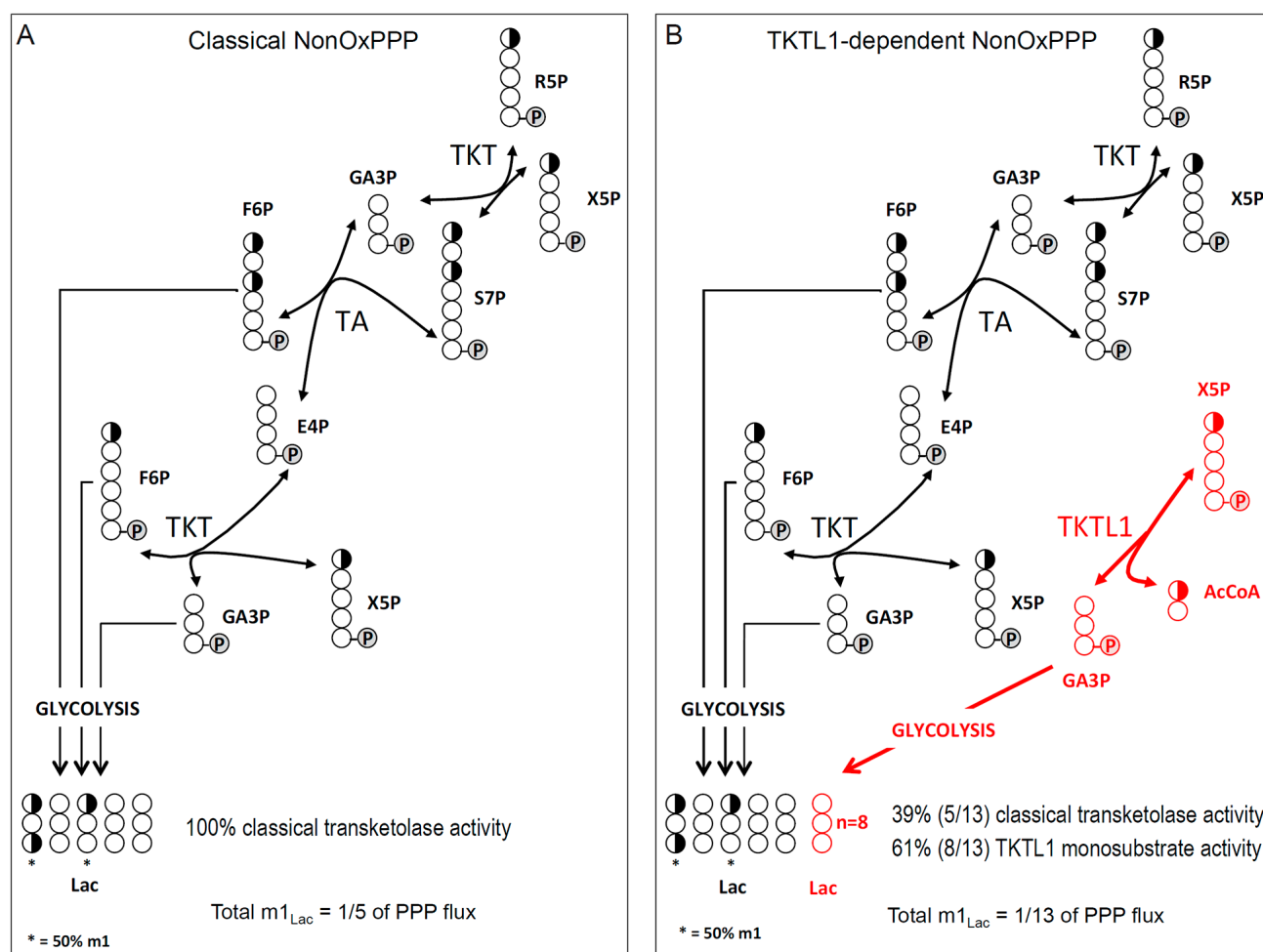


**Figure 7: Label distribution depending on the mechanism of reaction of the TKTL1.** Schematic representation of the classically accepted sequence of reactions of the non-oxPPP **A.**, and the proposed sequence of reactions for the non-oxPPP showing AcCoA production in the one-substrate reaction of TKTL1 (in red) **B.** Carbons are represented by circles. Half-filled circles represent carbons that have 50% chance of incorporating label from [1,2-<sup>13</sup>C<sub>2</sub>]-glucose; open circles represent unlabeled carbons. Circles containing P represent phosphate groups. R5P, ribose-5-phosphate; X5P, xylulose-5-phosphate; GA3P, glyceraldehyde-3-phosphate; S7P, sedoheptulose-7-phosphate; F6P, fructose-6-phosphate; E4P, erythrose-4-phosphate; AcCoA, acetyl-CoA; TKT, transketolase; TA, transaldolase; Lac, Lactate.



PPP contribute to the maintenance of redox homeostasis, our results suggest that the previously described role of TKTL1 in protecting cells against oxidative stress [38] is independent of its contribution to the overall transketolase activity.

Although our results suggest that TKTL1 affects cell metabolism via mechanisms that are either dependent or independent of its enzymatic activity, they also unambiguously show that TKTL1 has transketolase enzymatic activity, supporting previous reports [10, 20, 32], and refuting studies claiming that TKTL1 lacks enzymatic activity [39, 40]. In our studies, TKTL1 silencing lowered the overall cellular transketolase activity, supporting that TKTL1 cleaves a two-carbon fragment from a pentose-phosphate to generate GA3P. Failure to detect *in vitro* transketolase activity of an artificial TKT protein variant with a 38 amino acid deletion was used in previous studies as an argument against an intrinsic enzymatic function of TKTL1, although no experiments were performed with the wild-type TKTL1 protein [39]. We speculate that the lack of transketolase activity by this TKT deletion variant might be due to defective interactions with other cellular components or cofactors that may be required for its enzymatic activity. Alternatively, why TKTL1 activity is detected *in vivo*, but not *in vitro*, might be attributed to the weak binding of TKTL1 to its cofactor, thiamine diphosphate, which retains the two-carbon fragment upon cleavage of X5P until it is transferred to R5P.

Our characterization of the oncogenic role of TKTL1 also sheds light on two largely unexplained phenomena in cancer cell metabolism. First, the TKTL1 activity described here better reconciles with the proposed hypothetical reaction scheme [23]. Second, our observations may help resolve the outstanding enigma of how rapidly proliferating cells can boost lipid synthesis [41] when AcCoA production is limited by impaired

pyruvate production from phosphoenolpyruvate (because of PKM2 overexpression) [25, 26] and inhibition of PDH (which drives pyruvate to lactate, thereby reducing pyruvate entry into the TCA cycle) [27, 42, 43]. Taking into account that i) silencing of TKTL1 or ACLY in HCT116 cells reduced the expression of the corresponding protein to a similar extent (around 50%), and ii) the decrease in palmitate enrichment from labeled glucose was similar for both knock downs (around 40-60%), it can be estimated that a fully active TKTL1 can contribute to up to 50% of the flux from glucose to fatty acid synthesis. Indeed, our study shows that TKTL1 plays a significant role in the synthesis of fatty acids and phospholipids.

The observed enrichment of [1,2-<sup>13</sup>C<sub>2</sub>]-glucose in m1 lactate is consistent with the one-substrate reaction previously suggested by Coy *et al.* [8]. In this regard, the 38-amino acid segment in TKT missing in TKTL1 contains a critical histidine residue, homologous to His103 in the *S. cerevisiae* transketolase protein. Site-directed mutagenesis of this residue in the yeast transketolase converts its activity from the classical two-substrate reaction to a one-substrate reaction [44]. We speculate that, by analogy, the absence of the equivalent His residue in mammalian TKTL1 may favor the one-substrate reaction, whereby X5P is converted to GA3P and a two-carbon fragment. This fragment could be AcCoA or acetate (that subsequently generates AcCoA via acetyl-CoA synthetase 2) [45, 46]. Thus, TKTL1 may link the synthesis of nucleotide precursors (R5P) to the production of fatty acid precursors (AcCoA), providing an alternative explanation for how cancer cells can generate new lipids when AcCoA production from glucose metabolism is restricted. This TKTL1-specific one-substrate reaction would also explain why TKTL1 silencing in HCT116<sup>KD</sup> and PC-3M<sup>KD</sup> cells reduces cell proliferation, while not affecting overall transketolase activity. We thus speculate that the evolutionary removal in TKTL1 of the 38 amino

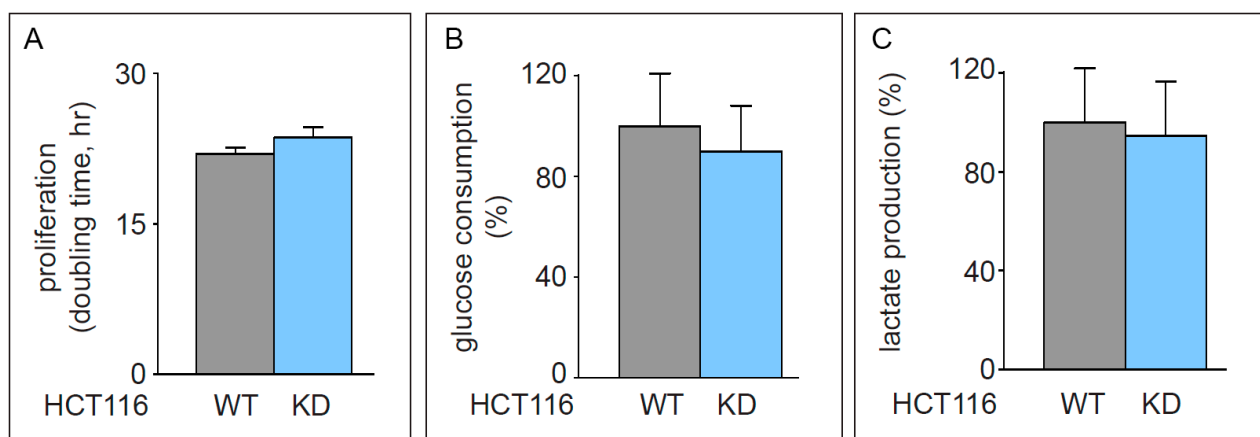


**Figure 8: Effect of ACLY knock down in HCT116 cells.** A. Proliferation assay (mean±SD; n=3; p=0.21) in HCT116<sup>WT</sup> and HCT116-ACLY<sup>KD</sup>. B. Glucose consumption (mean±SD; n=5; p=0.42). C. Lactate production (mean±SD; n=5; p=0.69) (mean±SD; n=5; p=0.40).

acid residues present in TKT, which includes the His residue equivalent to yeast His103, has created a new enzyme capable of catalyzing a one-substrate reaction that enables the fermentation of glucose to lactic acid and AcCoA even in the presence of oxygen.

Our study therefore shows that TKTL1 is an active transketolase that modulates the Warburg effect to provide energy and precursors for DNA replication and membrane biogenesis depending on its enzymatic activity. Moreover, our results suggest that TKTL1 controls redox homeostasis and protects cells against oxidative stress and apoptosis independent of its transketolase activity. Finally, we have shown that TKTL1 participates in the synthesis of lactosylceramides, a sphingolipid regulating cell survival, proliferation and angiogenesis [47, 48], and phosphatidylinositols, which activate PI3K/Akt/mTOR signaling [49].

In conclusion, we provide unprecedented evidence that TKTL1 confers a growth advantage to proliferating cells and is essential in cancer metabolic reprogramming, suggesting that TKTL1 might be a promising target for the design of future anti-cancer therapies.

## MATERIALS AND METHODS

### Chemicals and reagents

All chemicals were purchased from Sigma-Aldrich Co (St Louis, MO, USA), unless otherwise specified. Antibiotics (10,000 U/ml penicillin, 10,000 µg/ml streptomycin) were obtained from Gibco-BRL (Eggenstein, Germany), fetal calf serum (FCS) and trypsin-EDTA solution C (0.05% trypsin - 0.02% EDTA) from PAA Laboratories (Pasching, Austria). Stable [1,2-<sup>13</sup>C<sub>2</sub>]-D-glucose isotope was obtained with > 99% purity and 99% isotope enrichment for each carbon from Isotec Inc. (Miamisburg, OH). TRIzol™ reagent was obtained from Invitrogen (Paisley, UK). RNase was obtained from Roche Diagnostics (Mannheim, Germany). Phospholipid and sphingolipid standards were purchased from Sigma-Aldrich Co. (St. Louis, MO) (PC 34:0, PE 34:0, PG 34:0, PI 34:2, PS 34:0, LysoPC 17:0, Cer 12:0, GlcCer 12:0, LacCer 12:0 and SM 12:0) or Avanti Polar Lipids, Inc. (Alabaster, AL) (Cer 24:1 and sphinganine 17:0).

### Cell culture

Human THP-1 acute monocytic leukemia and human HCT116 colon carcinoma cells were obtained from the American Type Culture Collection (Manassas, VA, US). THP-1 WT and TKTL1<sup>KD</sup> cells were generated by Sirion Biotech GmbH (Munich, Germany). THP-1 and HCT116 cell lines were grown in RPMI 1640 culture medium supplemented with 10% heat-inactivated FCS and antibiotics: 100 U/ml penicillin and 100 µg/ml. HCT116

were grown in DMEM:HAM F12 (1:1), supplemented with 10% heat-inactivated FCS, 2 mM L-glutamine, 1 mM pyruvic acid 1% non-essential amino acids, 100 U/ml penicillin and 100 µg/ml streptomycin. PC-3M and PC-3S human prostatic adenocarcinoma sub-lines were generated as described in [50] and were grown in RPMI 1640 medium supplemented with 10% heat-inactivated FCS, 1 mM pyruvic acid, 1% non-essential amino acids, 100 U/ml penicillin, 100 µg/ml streptomycin and 200 µg/ml geneticin.

### RT-PCR

Total RNA was isolated from cultured cells (approximately 1-2 x 10<sup>6</sup> cells) using the TRIzol reagent (Roche Diagnostics). For quantitative RT-PCR, cDNA was synthesized from 1 µg of total RNA using random hexamers and M-MLV-reverse transcriptase (Invitrogen) and subjected to real-time PCR with specific TaqMan probes (Assays-on-demand TKTL1: Hs00202061\_m1; ACLY: Hs00153764\_m1; reference probe, PPIA: Hs99999904\_m1) (Applied Biosystems, Foster City, CA) on a ABI Prism 7700 Sequence Detector System (Applied Biosystems). All reactions were performed in triplicate. Fold changes in gene expression were calculated using the  $\Delta\Delta C_t$  method, using as PPIA as a reference.

### Silencing of TKTL1 and ACLY

Human TKTL1 and ACLY-specific siRNAs and non-targeting control duplexes (Thermo Scientific Dharmacon, Lafayette, CO, USA) were transfected using Metafectene (Biontex, Munich, Germany). The highest efficiency in TKTL1 silencing was accomplished with 5'-GGAGUUGCAUGUGGAAUGG-3' (catalog no. J-004736-06). For ACLY silencing a mixture of 4 siRNA was most effective (ON-TARGETplus SMARTpool: 5'-GCACGAAGUCACAAUCUUU-3', 5'-CGAGUGAAGUCGAUAAACA-3', 5'-GAGAGCAAUUCGAGAUUAC-3' and 5'-CCACUCCUCUGCUCGAUUA-3', catalog no. L-004915-00). RNA and protein expression assays were determined 72 and 96 h after transfection, respectively. Glucose consumption, lactate production and glutamate/glutamine variations were assessed 96 h post transfection. Transketolase activity was determined 96 and 120 h post transfection.

### Western blotting

Western blotting analyses were performed on cellular lysates (100 µl of lysis buffer was added per 10<sup>6</sup> cells, lysis buffer contained 20 mM Tris HCl pH 7.5, 1 mM dithiothreitol (DTT), 1 mM EDTA, 0.2 g/L Triton X-100, 0.2 g/L sodium deoxycholate, 0.2 mM PMSF (phenylmethylsulfonyl fluoride) and 1/1000

orthovanadate, 1/500 PMSF, 1/100 leupeptin and 1/100 aprotinin. Following addition of the lysis buffer, cells were sonicated for 5 min in ice-water bath at low intensity (40 kHz) and centrifuged at 4°C for 10 min at 20,000 x g. Samples (30 µg protein) were resolved by 12% SDS-PAGE, transferred to PVDF membranes (Bio-Rad, El Prat de Llobregat, Spain), membranes were blocked with 5% milk in PBS for 1 h at 20°C and incubated overnight at 4°C with primary antibodies diluted in Tris-buffered saline containing 0.1% Tween 20 (TBS-T). After washing, membranes were incubated with the secondary antibody for 1 h at 20°C. Visualization of specific bands was accomplished by chemiluminescence (Millipore, Billerica, MA) in a LAS-3000 imaging system (Fuji Photo Film, Tilburg, The Netherlands). Antibodies used were: mouse monoclonal anti-TKTL1 antibody (clone JFC12T10), rabbit anti-TKT antibody, rabbit polyclonal anti-ACLY antibody (catalogue no. 4332, Cell Signaling Technology). Loading control was performed by Western blotting analysis for actin using mouse monoclonal (MP Biomedicals, Santa Ana, CA) or rabbit polyclonal (Sigma-Aldrich) anti-actin antibodies.

### Cell proliferation

Cells were seeded in 6-well plates at a concentration of 75,000 cells per well and counted using a Scepter Handheld Automated Cell Counter (Millipore). THP-1<sup>WT</sup> and THP-1<sup>KD</sup> cells were seeded in 75 cm<sup>2</sup> flasks at a concentration of 200 x 10<sup>3</sup> cells/mL in a total volume of 15 mL medium. Every 24 h until 120 h an aliquot of 1 mL medium was removed and cells were counted. Duplication times were determined as the slope of the graph obtained by plotting the napierian logarithm of cell concentration (cells/mL) versus the incubation time in hours corresponding to the period of cellular exponential growth.

### TKT enzymatic activity

Fresh cell pellets containing approximately 5-10 x 10<sup>6</sup> cells were resuspended in lysis buffer (20 mM HEPES, pH 7.5, 10% glycerol, 0.4 mM NaCl, 10 mM EGTA, 5 mM EDTA, 0.4% Triton X-100, 25 mM NaF, 1 mM DTT, 0.4 mM Pefabloc SC, 20 µg/mL pepstatin), sonicated in ice-cold buffer (4°C) and immediately followed by centrifugation at 15,000 x g for 15 min at 4°C. The supernatant was used for the determination of enzyme activity with a Cobas Mira Plus analyzer (HORIBA ABX, Montpellier, France). Transketolase activity was determined as described [51]. Briefly, the TKT activity product, glyceraldehyde-3-phosphate, is isomerized to dihydroxyacetone-phosphate and its subsequent conversion to glycerol-phosphate produces 1 molecule of NADH that absorbs at 340 nm. Initially, 40 µL of sample were added to a cuvette containing 150 µL of buffer (50 mM Tris-HCl buffer, pH 7.6; 5 mM MgCl<sub>2</sub>; 0.1

mM thiamine pyrophosphate (TPP); 0.2 mM NADH; 0.2 U/mL triose phosphate isomerase and 0.2 U/mL glycerol dehydrogenase). The reaction mixture was kept at 37°C for 15 min in order to convert the trioses-phosphate into glycerol-phosphate. Finally, 75 µL of a solution containing 25 mM R5P and 25 mM X5P was transferred to the cuvette and absorbance at 340 nm was recorded for 5 min.

### Metabolite measurement

Glucose, lactate, glutamine and glutamate concentrations in media were determined as described [52, 53] using a Cobas Mira Plus instrument (Roche). Glutamine quantification was achieved by converting it to glutamate using glutaminase (Sigma-Aldrich). The isotopologue distribution of glucose, lactate, RNA ribose, glutamate and fatty acids after incubation with [1,2-<sup>13</sup>C<sub>2</sub>]-D-glucose (Isotec) was analyzed by GC-MS as described [54, 55] using a Shimadzu GCMS-QP2010 system (Duisburg, Germany).

### Amino acid quantification

Amino acid concentrations in cell culture medium were determined by ion-exchange chromatography with a Biochrom 30 amino acid analyzer (Pharmacia Biochrom Ltd, Cambridge, UK). 70 µL of 150 µM norleucine was used as an internal standard and added to 500 µL of medium. Solvent was evaporated to complete dryness using a Savant SpeedVac (Thermo Scientific, Waltham, MA, USA). The samples were redissolved in 500 µL lithium citrate buffer (pH 2.2), filtered through a 0.22 µm filter and 30 µL per sample injected onto the Biochrom 30 lithium system. A set of lithium citrate buffers were used as a mobile phase for separation for 115 min and post column derivatization with ninhydrin allowed amino acid quantification at 570 and 440 nm.

### Isotopologue analysis by GC-MS

For isotopologue distribution analysis, 3 x 10<sup>5</sup> cells/mL were seeded in 75 cm<sup>2</sup> Petri dishes in the presence of RPMI 1640 medium spiked with 10 mM of [1,2-<sup>13</sup>C<sub>2</sub>]-glucose (Sigma-Aldrich) (50% isotope enrichment), for 48 h. Following incubation, cells were counted with a Scepter Handheld Automated Cell Counter (Millipore) and centrifuged (1,500 rpm for 5 min). Medium was collected for glucose, lactate and glutamate/glutamine analysis, and cell pellets were frozen for RNA ribose and fatty acids analysis.

Glucose was isolated from 200 µL medium by ion-exchange chromatography and converted to its aldonitrile acetate derivative by adding 100 µL hydroxylamine in pyridine (2% wt) at 100°C for 30 min followed by 75 µL acetic anhydride at 100°C for 1 h. The reaction mixture was evaporated to complete dryness and redissolved in 50 to 200 µL of ethyl acetate. 1 µL of the derivatized product

was loaded to a GC-2010 gas chromatograph (Shimadzu) equipped with a HP-5MS capillary column (30 m length, 250  $\mu$ m diameter and 0.25  $\mu$ m film thickness), connected to a GCMSQP2010 mass selective detector (Shimadzu) [54]. *Lactate* was extracted from the medium by ethyl acetate after acidification with HCl and 1 mL ethyl acetate at 20°C. The propylamideheptafluorobutyric derivative of the lactate was prepared and analyzed as described [55]. *RNA ribose* was isolated by acid hydrolysis of cellular RNA after Trizol (Invitrogen) extraction from cell pellets. Ribose was derivatized to its aldonitrile acetate form by an analogous derivatization procedure as described for glucose. After derivatization, the reaction mixture was evaporated to complete dryness and redissolved in 50 to 200  $\mu$ L of ethyl acetate. *Glutamate* was isolated from 1 mL of cell medium using ion-exchange chromatography and converted to its n-trifluoroacetyl-n-butyl derivative by adding 200  $\mu$ L of butanolic HCl (0.4 N), the mixture incubated at 100°C for 1 h and dried under nitrogen stream. Next, 100  $\mu$ L methylene chloride and 25  $\mu$ L trifluoroacetic acid were added. The solution was kept at 20°C for 20 min and dried under nitrogen stream. The pellet was dissolved in 50 to 200  $\mu$ L methylene chloride and 1  $\mu$ L was injected for analysis [34, 55]. *Fatty acids* were extracted with methanol from the organic phase obtained during RNA isolation with Trizol (Invitrogen). Purified fatty acids were converted to their methyl ester derivatives by adding 200 to 500  $\mu$ L of methanolic HCl 0.5 N, heating at 70°C for 1 h, drying under nitrogen stream and dissolving in 200  $\mu$ L of hexane for injecting 1  $\mu$ L in the GC-MS, now equipped with a bpx70 (SGE) column (30 m length, 250  $\mu$ m diameter and 0.25  $\mu$ m film thickness).

## Lipidomic analysis

Two standard mixes of phospholipids (PL) and sphingolipids (SL) were prepared. The PL mix contained PC 34:0, PE 34:0, PG 34:0, PI 34:2, PS 34:0 and LysoPC 17:0 at a concentration of 20  $\mu$ M each. The SL mixture contained Cer 12:0, GlcCer 12:0, LacCer 12:0, SM 12:0 and sphinganine 17:0 at a concentration of 20  $\mu$ M each. These mixes were used as internal standards for PL and SL identification and quantification at a final concentration of 200 pmol/sample. Two pellets containing  $750 \times 10^3$  cells each were re-suspended in 100  $\mu$ L of milliQ water and 500  $\mu$ L pure methanol (MeOH), these suspensions were transferred to glass vials. 250  $\mu$ L chloroform ( $\text{CHCl}_3$ ) was added to obtain an extraction solvent MeOH: $\text{CHCl}_3$ : $\text{H}_2\text{O}$  (2:1:0.4). 10  $\mu$ L of PL or SL standard mix was added and lipids were extracted overnight at 48°C. For sphingolipid analysis, 75  $\mu$ L of 1 M potassium hydroxide (KOH) dissolved in MeOH was added and samples were sonicated. After 2 h of incubation at 37°C, 75  $\mu$ L of 1 M acetic acid was added. Following extraction, PL and SL samples were dried

under nitrogen stream and stored at -20°C until further usage. Prior to analysis on an UPLC-MS, samples were dissolved in 500  $\mu$ L MeOH and transferred to Eppendorf tubes. The volume was reduced by evaporation under gentle nitrogen steam to a final volume of 150  $\mu$ L MeOH, prior to analysis samples were centrifuged at 10,000  $\times$  g for 3 min and 150  $\mu$ L of supernatant was infused into the UPLC. The liquid chromatography–mass spectrometer (Waters Acquity UPLC system, connected to a Waters LCT Premier orthogonal accelerated time of flight mass spectrometer; Waters, Millford, MA) was operated in positive electrospray ionisation mode. Full scan spectra from 50 to 1,500 Da were acquired and individual spectra were summed to produce data points every 0.2 s. Mass accuracy and reproducibility were maintained by using an independent reference spray via LockSpray interference. The analytical column, maintained at 30°C, was a 100  $\times$  2.1 mm id, 1.7  $\mu$ m C8 Acquity UPLC BEH (Waters). The mobile phase consisted of solvent A: MeOH/ $\text{H}_2\text{O}$ /HCOOH (74:25:1 v:v:v); and solvent B: MeOH/HCOOH (99:1 v:v), both containing 5 mM ammonium formate. A gradient was programmed - 0.0 min, 80% B; 3 min, 90% B; 6 min, 90% B; 15 min, 99% B; 18 min, 99% B; 20 min, 80% B; 22 min, 80% B, with a 300  $\mu$ L/min flow rate. Quantification was carried out using the ion chromatogram extracted for each compound in 50 mDa windows. The linear dynamic range was determined by injecting standard mixtures. Positive identification of compounds was based on the accurate mass measurement with an error < 5 ppm and its LC retention time, compared to that of a standard ( $\pm$  2%). Lipid species were assigned from the m/z values detected in the MS using the MassLynx software (v4.1 SCN627 Waters). Positive ionization allowed detection of PC, PC-pmg, Lyso-PC and Lyso-PC-pmg from the phospholipid extract and Cer, dihydroceramides, SM, dihydrosphingomyelins, GlcCer, glucosyldihydroceramides, LacCer and lactosyldihydroceramides from the sphingolipid extract. Negative ionization mode allowed detecting the rest of phospholipid classes: PE, PE-pmg, Lyso-PE, Lyso-PE-pmg, PS, Lyso-PS and PI.

## Statistical analysis

*In vitro* experiments were performed in triplicate for each treatment in at least two independent experiments. Mass spectrometric analyses were carried out in three independent 1  $\mu$ L injections of each sample by the automatic sampler in a linear set-up. Raw data were considered valid only if the sample deviation was < 1% of the normalized peak intensity. Statistical analyses were performed using the parametric unpaired, two-tailed independent sample Student's *t*-test, assuming normality of distribution and homogeneity of variance based on past experience in similar measurements [56, 57]. When a family of statistical hypotheses was tested in the same

series of experiments, the Holm method for P-value adjustment was used [58].  $P < 0.05$  (\*) was considered statistically significant.

## ACKNOWLEDGMENTS

Authors acknowledge Dr. Vitaly Selivanov (Department of Biochemistry and Molecular Biomedicine, Faculty of Biology, Universitat de Barcelona) for his help in the statistical analyses performed in the manuscript.

## CONFLICTS OF INTEREST

JF Coy is a shareholder of Zyagnum AG (Frankfurt am Main, Germany) and TAVARGENIX GmbH, (Frankfurt am Main, Germany). All other authors declare no conflicts of interest.

## GRANT SUPPORT

This work was supported by grants to M.C. (Agència de Gestió d'Ajuts Universitaris i de Recerca (AGAUR) – Generalitat de Catalunya, 2014SGR1017; ICREA Academia from the ICREA foundation; and MINECO-European Commission FEDER – Una manera de hacer Europa, SAF2014-56059-R), T.M.T. (MINECO-European Commission FEDER – Una manera de hacer Europa, SAF2015-66984-C2-1-R; and Xarxa de Referència en Biotecnologia) and P.C. (Research Foundation-Flanders (FWO), Belgian Science Policy grant (IUAP P7/03); long-term structural Methusalem funding by the Flemish Government; European Research Council (ERC) Advanced Research Grant (EU-ERC269073); and AXA Research Fund).

## REFERENCES

1. Hanahan D, Weinberg RA. Hallmarks of cancer: the next generation. *Cell*. 2011; 144:646-674.
2. Kroemer G, Pouyssegur J. Tumor cell metabolism: cancer's Achilles' heel. *Cancer cell*. 2008; 13:472-482.
3. Schulze A, Harris AL. How cancer metabolism is tuned for proliferation and vulnerable to disruption. *Nature*. 2012; 491:364-373.
4. Furuta E, Okuda H, Kobayashi A, Watabe K. Metabolic genes in cancer: their roles in tumor progression and clinical implications. *Biochim Biophys Acta*. 2010; 1805:141-152.
5. Smith IM, Glazer CA, Mithani SK, Ochs MF, Sun W, Bhan S, Vostrov A, Abdullaev Z, Lobanekov V, Gray A, Liu C, Chang SS, Ostrow KL, Westra WH, Begum S, Dhara M, et al. Coordinated activation of candidate proto-oncogenes and cancer testis antigens via promoter demethylation in head and neck cancer and lung cancer. *PLoS One*. 2009; 4:e4961.
6. Patra KC, Hay N. The pentose phosphate pathway and cancer. *Trends Biochem Sci*. 2014; 39:347-354.
7. Sun W, Liu Y, Glazer CA, Shao C, Bhan S, Demokan S, Zhao M, Rudek MA, Ha PK, Califano JA. TKTL1 is activated by promoter hypomethylation and contributes to head and neck squamous cell carcinoma carcinogenesis through increased aerobic glycolysis and HIF1alpha stabilization. *Clin Cancer Res*. 2010; 16:857-866.
8. Coy JF, Dressler D, Wilde J, Schubert P. Mutations in the transketolase-like gene TKTL1: clinical implications for neurodegenerative diseases, diabetes and cancer. *Clin Lab*. 2005; 51:257-273.
9. Coy JF, Dubel S, Kioschis P, Thomas K, Micklem G, Delius H, Poustka A. Molecular cloning of tissue-specific transcripts of a transketolase-related gene: implications for the evolution of new vertebrate genes. *Genomics*. 1996; 32:309-316.
10. Chen H, Yue JX, Yang SH, Ding H, Zhao RW, Zhang S. Overexpression of transketolase-like gene 1 is associated with cell proliferation in uterine cervix cancer. *J Exp Clin Cancer Res*. 2009; 28:43.
11. Langbein S, Zerilli M, Zur Hausen A, Staiger W, Rensch-Boschert K, Lukan N, Popa J, Ternullo MP, Steidler A, Weiss C, Grobholz R, Willeke F, Alken P, Stassi G, Schubert P, Coy JF. Expression of transketolase TKTL1 predicts colon and urothelial cancer patient survival: Warburg effect reinterpreted. *Br J Cancer*. 2006; 94:578-585.
12. Volker HU, Hagemann C, Coy J, Wittig R, Sommer S, Stojic J, Haubitz I, Vince GH, Kammerer U, Monoranu CM. Expression of transketolase-like 1 and activation of Akt in grade IV glioblastomas compared with grades II and III astrocytic gliomas. *Am J Clin Pathol*. 2008; 130:50-57.
13. Zerilli M, Amato MC, Martorana A, Cabibi D, Coy JF, Cappello F, Pompei G, Russo A, Giordano C, Rodolico V. Increased expression of transketolase-like-1 in papillary thyroid carcinomas smaller than 1.5 cm in diameter is associated with lymph-node metastases. *Cancer*. 2008; 113:936-944.
14. Diaz-Moralli S, Tarrado-Castellarnau M, Alenda C, Castells A, Cascante M. Transketolase-like 1 expression is modulated during colorectal cancer progression and metastasis formation. *PLoS one*. 2011; 6:e25323.
15. Kayser G, Siemel W, Kubitz B, Mattern D, Stickeler E, Passlick B, Werner M, Zur Hausen A. Poor outcome in primary non-small cell lung cancers is predicted by transketolase TKTL1 expression. *Pathology*. 2011; 43:719-724.
16. Schwaab J, Horisberger K, Strobel P, Bohn B, Gencer D, Kahler G, Kienle P, Post S, Wenz F, Hofmann WK, Hofheinz RD, Erben P. Expression of Transketolase like gene 1 (TKTL1) predicts disease-free survival in patients with locally advanced rectal cancer receiving neoadjuvant chemoradiotherapy. *BMC Cancer*. 2011; 11:363.
17. Xu X, Zur Hausen A, Coy JF, Lochelt M. Transketolase-like protein 1 (TKTL1) is required for rapid cell growth and full viability of human tumor cells. *Int J Cancer*. 2009; 124:1330-1337.

18. Hartmannsberger D, Mack B, Eggert C, Denzel S, Stepp H, Betz CS, Gires O. Transketolase-like protein 1 confers resistance to serum withdrawal *in vitro*. *Cancer Lett.* 2011; 300:20-29.
19. Wanka C, Steinbach JP, Rieger J. Tp53-induced glycolysis and apoptosis regulator (TIGAR) protects glioma cells from starvation-induced cell death by up-regulating respiration and improving cellular redox homeostasis. *J Biol Chem.* 2012; 287:33436-33446.
20. Zhao F, Mancuso A, Bui TV, Tong X, Gruber JJ, Swider CR, Sanchez PV, Lum JJ, Sayed N, Melo JV, Perl AE, Carroll M, Tuttle SW, Thompson CB. Imatinib resistance associated with BCR-ABL upregulation is dependent on HIF-1 $\alpha$ -induced metabolic reprogramming. *Oncogene.* 2010; 29:2962-2972.
21. Hu LH, Yang JH, Zhang DT, Zhang S, Wang L, Cai PC, Zheng JF, Huang JS. The TKTL1 gene influences total transketolase activity and cell proliferation in human colon cancer LoVo cells. *Anticancer Drugs.* 2007; 18:427-433.
22. Yuan W, Wu S, Guo J, Chen Z, Ge J, Yang P, Hu B, Chen Z. Silencing of TKTL1 by siRNA inhibits proliferation of human gastric cancer cells *in vitro* and *in vivo*. *Cancer Biol Ther.* 2010; 9:710-716.
23. Horecker BL, Gibbs M, Klenow H, Smyrniotis PZ. The mechanism of pentose phosphate conversion to hexose monophosphate. I. With a liver enzyme preparation. *J Biol Chem.* 1954; 207:393-403.
24. Yevenes A, Frey PA. Cloning, expression, purification, cofactor requirements, and steady state kinetics of phosphoketolase-2 from *Lactobacillus plantarum*. *Bioorg Chem.* 2008; 36:121-127.
25. Anastasiou D, Pouligiannis G, Asara JM, Boxer MB, Jiang JK, Shen M, Bellinger G, Sasaki AT, Locasale JW, Auld DS, Thomas CJ, Vander Heiden MG, Cantley LC. Inhibition of pyruvate kinase M2 by reactive oxygen species contributes to cellular antioxidant responses. *Science.* 2011; 334:1278-1283.
26. Hamanaka RB, Chandel NS. Cell biology. Warburg effect and redox balance. *Science.* 2011; 334:1219-1220.
27. Kim JW, Tchernyshyov I, Semenza GL, Dang CV. HIF-1-mediated expression of pyruvate dehydrogenase kinase: a metabolic switch required for cellular adaptation to hypoxia. *Cell metabolism.* 2006; 3:177-185.
28. Miccheli A, Tomassini A, Puccetti C, Valerio M, Peluso G, Tuccillo F, Calvani M, Manetti C, Conti F. Metabolic profiling by <sup>13</sup>C-NMR spectroscopy: [1,2-<sup>13</sup>C<sub>2</sub>]glucose reveals a heterogeneous metabolism in human leukemia T cells. *Biochimie.* 2006; 88:437-448.
29. Dang CV. Glutaminolysis: supplying carbon or nitrogen or both for cancer cells? *Cell Cycle.* 2010; 9:3884-3886.
30. Metallo CM, Gameiro PA, Bell EL, Mattaini KR, Yang J, Hiller K, Jewell CM, Johnson ZR, Irvine DJ, Guarente L, Kelleher JK, Vander Heiden MG, Iliopoulos O, Stephanopoulos G. Reductive glutamine metabolism by IDH1 mediates lipogenesis under hypoxia. *Nature.* 2012; 481:380-384.
31. Mullen AR, Wheaton WW, Jin ES, Chen PH, Sullivan LB, Cheng T, Yang Y, Linehan WM, Chandel NS, DeBerardinis RJ. Reductive carboxylation supports growth in tumour cells with defective mitochondria. *Nature.* 2012; 481:385-388.
32. Zhang S, Yang JH, Guo CK, Cai PC. Gene silencing of TKTL1 by RNAi inhibits cell proliferation in human hepatoma cells. *Cancer Lett.* 2007; 253:108-114.
33. Feyen O, Coy JF, Prasad V, Schierl R, Saenger J, Baum RP. EDIM-TKTL1 blood test: a noninvasive method to detect upregulated glucose metabolism in patients with malignancies. *Future Oncol.* 2012; 8:1349-1359.
34. Boros LG, Cascante M, Lee WN. Metabolic profiling of cell growth and death in cancer: applications in drug discovery. *Drug Discov Today.* 2002; 7:364-372.
35. Locasale JW, Grassian AR, Melman T, Lyssiotis CA, Mattaini KR, Bass AJ, Heffron G, Metallo CM, Muranen T, Sharfi H, Sasaki AT, Anastasiou D, Mullarky E, Vokes NI, Sasaki M, Beroukhim R, et al. Phosphoglycerate dehydrogenase diverts glycolytic flux and contributes to oncogenesis. *Nat Genet.* 2011; 43:869-874.
36. Tong J, Xie G, He J, Li J, Pan F, Liang H. Synergistic antitumor effect of dichloroacetate in combination with 5-fluorouracil in colorectal cancer. *J Biomed Biotechnol.* 2011; 2011:740564.
37. Vaughn AE, Deshmukh M. Glucose metabolism inhibits apoptosis in neurons and cancer cells by redox inactivation of cytochrome c. *Nat Cell Biol.* 2008; 10:1477-1483.
38. Bentz S, Pesch T, Wolfram L, de Valliere C, Leucht K, Fried M, Coy JF, Hausmann M, Rogler G. Lack of transketolase-like (TKTL) 1 aggravates murine experimental colitis. *Am J Physiol Gastrointest Liver Physiol.* 2011; 300:G598-607.
39. Meshalkina LE, Drutsa VL, Koroleva ON, Solovjeva ON, Kochetov GA. Is transketolase-like protein, TKTL1, transketolase? *Biochim Biophys Acta.* 2013; 1832:387-390.
40. Schneider S, Ludtke S, Schroder-Tittmann K, Wechsler C, Meyer D, Tittmann K. A delta38 deletion variant of human transketolase as a model of transketolase-like protein 1 exhibits no enzymatic activity. *PLoS One.* 2012; 7:e48321.
41. Schug ZT, Frezza C, Galbraith LC, Gottlieb E. The music of lipids: how lipid composition orchestrates cellular behaviour. *Acta Oncol.* 2012; 51:301-310.
42. Hitosugi T, Fan J, Chung TW, Lythgoe K, Wang X, Xie J, Ge Q, Gu TL, Polakiewicz RD, Roesel JL, Chen GZ, Boggon TJ, Lonial S, Fu H, Khuri FR, Kang S, et al. Tyrosine phosphorylation of mitochondrial pyruvate dehydrogenase kinase 1 is important for cancer metabolism. *Mol Cell.* 2011; 44:864-877.
43. Lu CW, Lin SC, Chen KF, Lai YY, Tsai SJ. Induction of pyruvate dehydrogenase kinase-3 by hypoxia-inducible factor-1 promotes metabolic switch and drug resistance. *J Biol Chem.* 2008; 283:28106-28114.

44. Selivanov VA, Kovina MV, Kochevova NV, Meshalkina LE, Kochetov GA. Kinetic study of the H103A mutant yeast transketolase. *FEBS Lett.* 2004; 567:270-274.
45. Comerford SA, Huang Z, Du X, Wang Y, Cai L, Witkiewicz AK, Walters H, Tantawy MN, Fu A, Manning HC, Horton JD, Hammer RE, McKnight SL, Tu BP. Acetate dependence of tumors. *Cell.* 2014; 159:1591-1602.
46. Mashimo T, Pichumani K, Vemireddy V, Hatanpaa KJ, Singh DK, Sirasanagandla S, Nannepaga S, Piccirillo SG, Kovacs Z, Foong C, Huang Z, Barnett S, Mickey BE, DeBerardinis RJ, Tu BP, Maher EA, et al. Acetate is a bioenergetic substrate for human glioblastoma and brain metastases. *Cell.* 2014; 159:1603-1614.
47. Gong N, Wei H, Chowdhury SH, Chatterjee S. Lactosylceramide recruits PKC $\alpha$ /epsilon and phospholipase A2 to stimulate PECAM-1 expression in human monocytes and adhesion to endothelial cells. *Proc Natl Acad Sci U S A.* 2004; 101:6490-6495.
48. Kolmakova A, Rajesh M, Zang D, Pili R, Chatterjee S. VEGF recruits lactosylceramide to induce endothelial cell adhesion molecule expression and angiogenesis *in vitro* and *in vivo*. *Glycoconj J.* 2009; 26:547-558.
49. Chalhoub N, Baker SJ. PTEN and the PI3-kinase pathway in cancer. *Annu Rev Pathol.* 2009; 4:127-150.
50. Celia-Terrassa T, Meca-Cortes O, Mateo F, de Paz AM, Rubio N, Arnal-Estape A, Ell BJ, Bermudo R, Diaz A, Guerra-Rebollo M, Lozano JJ, Estaras C, Ulloa C, Alvarez-Simon D, Mila J, Vilella R, et al. Epithelial-mesenchymal transition can suppress major attributes of human epithelial tumor-initiating cells. *J Clin Invest.* 2012; 122:1849-1868.
51. Obiol-Pardo C, Alcarraz-Vizan G, Cascante M, Rubio-Martinez J. Diphenyl urea derivatives as inhibitors of transketolase: a structure-based virtual screening. *PLoS One.* 2012; 7:e32276.
52. Gutmann I, Wahlefeld AW. L-(+)-Lactate: Determination with lactate dehydrogenase and NAD. In: Bergmeyer HU, ed. *Methods of Enzymatic Analysis* (New York: Academic Press). 1974; 1464-1468.
53. Kunst A, Draeger B, Ziegenhorn J. D-Glucose. UV-methods with hexokinase and glucose 6-phosphate dehydrogenase. In: Bergmeyer HU, Bergmeyer J, Grassl M, eds. *Methods of Enzymatic Analysis* (Weinheim: Verlag Chemie). 1984; 163-172.
54. Alcarraz-Vizan G, Boren J, Lee WN, Cascante M. Histone deacetylase inhibition results in a common metabolic profile associated with HT29 differentiation. *Metabolomics.* 2010; 6:229-237.
55. Lee WN, Boros LG, Puigjaner J, Bassilian S, Lim S, Cascante M. Mass isotopomer study of the nonoxidative pathways of the pentose cycle with [1,2- $^{13}C_2$ ]glucose. *Am J Physiol.* 1998; 274:E843-851.
56. Fan TW, Lane AN, Higashi RM, Farag MA, Gao H, Bousamra M, Miller DM. Altered regulation of metabolic pathways in human lung cancer discerned by ( $^{13}C$ ) stable isotope-resolved metabolomics (SIRM). *Mol Cancer.* 2009; 8:41.
57. Le A, Lane AN, Hamaker M, Bose S, Gouw A, Barbi J, Tsukamoto T, Rojas CJ, Slusher BS, Zhang H, Zimmerman LJ, Liebler DC, Slebos RJ, Lorkiewicz PK, Higashi RM, Fan TW, et al. Glucose-independent glutamine metabolism via TCA cycling for proliferation and survival in B cells. *Cell metabolism.* 2012; 15:110-121.
58. Holm S. A simple sequentially rejective multiple test procedure. *Scand J Statistics.* 1979; 6:65-70.